

2018

Residual Strength of Composite Materials After Exposure to Blast Loading

Monica L. Black
University of Rhode Island, monicab1@vt.edu

Follow this and additional works at: <https://digitalcommons.uri.edu/theses>

Terms of Use

All rights reserved under copyright.

Recommended Citation

Black, Monica L., "Residual Strength of Composite Materials After Exposure to Blast Loading" (2018).
Open Access Master's Theses. Paper 1186.
<https://digitalcommons.uri.edu/theses/1186>

This Thesis is brought to you by the University of Rhode Island. It has been accepted for inclusion in Open Access Master's Theses by an authorized administrator of DigitalCommons@URI. For more information, please contact digitalcommons-group@uri.edu. For permission to reuse copyrighted content, contact the author directly.

RESIDUAL STRENGTH OF COMPOSITE MATERIALS

AFTER EXPOSURE TO BLAST LOADING

BY

MONICA L. BLACK

A THESIS SUBMITTED IN PARTIAL FULFILLMENT OF THE

REQUIREMENTS FOR THE DEGREE OF

MASTER OF SCIENCE

IN

MECHANICAL ENGINEERING AND APPLIED MECHANICS

UNIVERSITY OF RHODE ISLAND

2018

MASTER OF SCIENCE THESIS
OF
MONICA L. BLACK

APPROVED:

Thesis Committee:

Major Professor Arun Shukla

David Taggart

Jason Dahl

Nasser H. Zawia
DEAN OF THE GRADUATE SCHOOL

UNIVERSITY OF RHODE ISLAND
2018

ABSTRACT

This research investigates the effects of shock loading on a composite structure's compressive residual strength. The research develops a methodology for evaluating and quantifying such damage using non-destructive imaging technologies, and develops a prediction equation for compressive residual strength of the damaged composite structure.

Experiments and imaging of Cyply 1002 glass-fiber/epoxy laminate panels were conducted at the University of Rhode Island (URI) and the Naval Undersea Warfare Center Division, Newport (NUWCDIVNPT), respectively. Controlled air blast experiments were conducted using the shock tube at URI's Dynamic Photomechanics Laboratory (DPML), inducing non-catastrophic damage on the panels. 3D Digital Image Correlation (DIC) was used to measure the transient response of the composite panels during blast loading, as well as material characterization and residual strength experiments. To evaluate the shock-induced damage in each composite panel, Terahertz (THz) and Flash Infrared Thermography (FIRT) were used to non-destructively obtain through-thickness images of the specimens before and after damage.

The results of the research show that THz and FIRT imaging can be used to quantify internal damage in a composite laminate after shock loading. Additionally, residual strength experiments show that increased shock damage causes a reduction in compressive residual strength. An analytical relationship was developed using MATLAB to predict the residual strength of a composite panel as a function of a combined damage parameter.

ACKNOWLEDGMENTS

It is with a grateful heart that I would like to thank the following people for making this research possible. First and foremost, I would like to thank my advisor Dr. Arun Shukla for welcoming me into the DPML, and encouraging me to think critically about my work. His technical guidance has helped me to understand, improve, and gain confidence in the quality of my research. I would also like to express my gratitude toward Dr. James LeBlanc of NUWCDIVNPT, who—in my first month of work—helped me find an advisor at URI and a path for completing my Master’s while working full-time. Dr. LeBlanc has been an exceptional educational mentor, and has introduced me to the world of scientific research, for which I will be forever grateful.

I would also like to thank Dr. Patric Lockhart of NUWCDIVNPT for his expertise and support with the THz and FIRT imaging. I am thankful to my colleagues in Code 4021, for developing my skills and passion for mechanical engineering, which helped me succeed in my coursework and thesis.

I would like to thank Dr. David Taggart and Dr. Jason Dahl for serving as my committee members, as well as the mechanical engineering department and staff for helping me in the machine shop, and helping me to never miss a paperwork deadline.

A special thanks goes out to my lab mates—Shyamal, Carlos, Koray, Chris, Irine, Prathamesh, Nidhi, Max, and Taylor—for making me a part of the DPML family, constantly asking questions, sharing their expertise, and making me laugh even when I was stressed. In addition to the technical depth they helped me find, I will always appreciate our traditions—including Thai Friday, coffee runs, and the fitness challenge.

I would like to acknowledge NUWCDIVNPT's financial support, provided through the Internal Investment Program (Section 219R funding) and the Fellowship Program. I am grateful to have an employer that invests in the education of its people, and provides such ample opportunities for me to use the education I have worked so hard to attain.

I would like to thank Adam, Chelsea, Jess, Sarah, Linley, and Shannon, among others—who have helped me maintain a work-life balance by encouraging me to pursue my education, but also joining me for much-needed vacations.

Last but not least, I would like to thank my parents Seth and Margo, and my sisters Danya and Miranda, for providing unconditional love and support as I completed my studies and pursued my career. I am unbelievably grateful to have such a strong and loving family just across the bridge.

For my family, and those that have made me feel like family

TABLE OF CONTENTS

ABSTRACT.....	ii
ACKNOWLEDGMENTS	iii
DEDICATION	v
TABLE OF CONTENTS.....	vi
LIST OF TABLES	viii
LIST OF FIGURES	ix
INTRODUCTION	1
MATERIAL STUDIED	5
RESEARCH OUTLINE	6
MATERIAL CHARACTERIZATION EXPERIMENTS	11
SHOCK LOADING EXPERIMENTS	18
IMAGING SYSTEMS AND DAMAGE QUANTIFICATION.....	25
RESIDUAL STRENGTH EXPERIMENTS	38
RELATIONSHIP BETWEEN DAMAGE AND RESIDUAL STRENGTH	44
CONCLUSIONS.....	50
LIST OF REFERENCES	52
APPENDIX A: PANEL IMAGES BEFORE, DURING, AND AFTER SHOCK	
TUBE EXPERIMENTS.....	55
APPENDIX B: TERAHERTZ (THZ) AND FLASH INFRARED THERMOGRAPHY	
(FIRT) IMAGES FOR ALL PANELS	65

APPENDIX C: ALTERNATIVE METHOD FOR CALCULATING THE COMBINED DAMAGE PARAMETER.....	78
APPENDIX D: MATLAB CODE FOR DETERMINING PREDICTION EQUATIONS.....	83
BIBLIOGRAPHY	88

LIST OF TABLES

TABLE	PAGE
Table 1. Mechanical properties of crossply and isotropic Cyply 1002.....	17
Table 2. Blast pressures and out-of-plane displacements for shock tube experiments	21
Table 3. Damage quantities for all subpanels determined through THz and FIRT	37
Table 4. Compressive residual strengths, σ_R , for all subpanels	43

LIST OF FIGURES

FIGURE	PAGE
Figure 1. Research approach	6
Figure 2. Diagram of the shock tube facility.....	8
Figure 3. Shock tube facility in the Dynamic Photomechanics Laboratory	8
Figure 4. Tensile specimen with emery cloth tabs, painted for DIC.....	12
Figure 5. INSTRON 3366 set up for Four-Point-Bend tests.....	13
Figure 6. (a) Front view of compression fixture with specimen painted for DIC [3], and (b) side view of compression fixture, showing empty specimen grooves....	14
Figure 7. Tensile Test Setup (left) and DIC Strain Contour of Specimen Failure (right)	16
Figure 8. Flexure test setup (left) and DIC strain contour of specimen failure (right)	16
Figure 9. Compression test setup (left) and DIC strain contour of specimen failure (right).....	17
Figure 10. (a) Schematic of mounting fixture and (b) composite panel mounted in front of shock tube muzzle	19
Figure 11. Arrangement of panel and Lexan windows for high speed photography..	20
Figure 12. Pressure profiles from shock tube experiments—crossply and isotropic panels.....	22
Figure 13. Panel 60-2i before (left), during (middle), and after (right) blast load.....	23
Figure 14. Panel 60-2i maximum out-of-plane displacement (W) during blast	23
Figure 15. Damage in panel 60-2i after blast loading—front face (left) and side (right)	

.....	24
Figure 16. FIRT imaging of damaged composite panel.....	26
Figure 17. THz system scanning composite panel.....	28
Figure 18. Behavior of THz waves through normal and defected composite material [19].....	28
Figure 19. (a) Representation of a damaged composite panel, and THz post-processing image types: (b) signal intensity map of x-y plane and (c) depth scan in the x-z plane	29
Figure 20. Panel 60-2i (top) cut into three 101.6 x 152.4 mm subpanels (bottom)	31
Figure 21. FIRT TSR image of panel 60-7i showing: a) orientation of fibers and ply 1 removal, b) major cracks, c) internal delamination, and d) back face speckle pattern.....	32
Figure 22. Panel 60-7i THz images—signal intensity map (left) and three depth scans (right) showing depth and location of cracks and delamination	33
Figure 23. Panel 60-7i damage quantification using a THz row depth scan (bottom) aligned with a signal intensity map (top)	34
Figure 24. THz images of center region of 60-7i :surface contour map (left) indicating slope of the panel surface, and internal surface map (right) showing delamination at the internal surfaces only.....	35
Figure 25. Subpanel cut and speckled for residual strength testing with DIC	38
Figure 26. Compressive residual strength fixture mounted on INSTRON 5585	39
Figure 27. Residual strength test setup with speckled subpanel mounted	40
Figure 28. End-crushing from residual strength test on low-damage subpanel 60-2c (c)	

.....	41
Figure 29. Subpanel 60-2i (c) before (left) and after (right) residual strength test, showing an acceptable failure mode initiating at damage location.....	41
Figure 30. Load-displacement curves for residual strength tests of subpanels 60-2i (c) and 60-2c (c) showing acceptable and unacceptable failure modes	42
Figure 31. Individual damage quantities plotted against residual strength with calculated correlations and linear best-fit lines	45
Figure 32. Scatter plot of combined damage parameter, $[d_c]$, versus residual strength, σ_R	47
Figure 33. 60-1c Panel images before and during blast using high speed cameras	56
Figure 34. Maximum out-of-plane displacement for 60-1c	56
Figure 35. 60-1c damaged after blast loading (front, back).....	56
Figure 36. 60-2c Panel images before, during, and after blast using high speed cameras	57
Figure 37. Maximum out-of-plane displacement for 60-2c	57
Figure 38. 60-2c damaged after blast loading (front, back).....	57
Figure 39. 60-5c panel images before, during, and after blast using high speed cameras	58
Figure 40. Maximum out-of-plane displacement for 60-5c	58
Figure 41. 60-5c damage after blast loading (front, back).....	58
Figure 42. 60-7c panel images before, during, and after blast using high speed cameras	59
Figure 43. maximum out-of-plane displacement for 60-7c	59

Figure 44. 60-9c panel images before, during, and after blast using high speed cameras	60
Figure 45. Maximum out-of-plane displacement for 60-9c	60
Figure 46. 60-1i panel images before and during blast using high speed cameras	61
Figure 47. Maximum out-of-plane displacement for 60-1i.....	61
Figure 48. 60-1i damage after blast loading (front, back).....	61
Figure 49. 60-2i panel images before and during blast using high speed cameras	62
Figure 50. Maximum out-of-plane displacement for 60-2i.....	62
Figure 51. 60-2i damage after blast loading (front, back, side)	62
Figure 52. 60-4i panel images before, during, and after blast using high speed cameras	63
Figure 53. Maximum out-of-plane displacement for 60-4i.....	63
Figure 54. 60-7i panel images before, during, and after blast using high speed cameras	64
Figure 55. Maximum out-of-plane displacement for 60-7i.....	64

INTRODUCTION

The research investigates the effects of shock damage on a composite structure's compressive residual strength. Through experimental techniques and non-destructive imaging technologies, the research develops a methodology for evaluating and quantifying such damage, and develops a prediction equation for compressive residual strength as a function of quantified damage.

Within the marine and aerospace communities, there is an interest in using composite materials for the design of structures, coatings, and vehicles. Composite materials offer lower maintenance costs, reduced electromagnetic and radar signatures, and high strength-to-weight ratios. However, the ability of these advanced materials to retain structural functionality after a shock event is not well understood, driving composite structures to require conservative designs with much higher safety factors than their metallic counterparts. Data on the residual strength of composite materials will improve the design of composite structures that may be exposed to blast loading.

Previous studies have characterized advanced composite materials [1] and examined the dynamic response of composite structures [2-4] under blast loading, allowing for improved designs using these advanced materials. Furthermore, recent studies have looked beyond the dynamic response, evaluating the residual strength of composite materials after exposure to dynamic loads such as impact, fatigue, and elevated temperatures. However, a knowledge gap exists for the residual strength of composite materials following a blast event.

The residual strength of composite materials after impact damage has been researched for many decades. These studies often have military or commercial aircraft applications; however, they also provide valuable data for naval applications. Kamala Kannan, et al. [5] created an inherent flaw model to compare the residual strength of composite laminate panels to its known fracture data in the form of holes and cracks. Kannan's research identified a reduction in strength of composite laminates after impact loading. Petit, et al. [6] studied advanced composite structures damaged by low velocity impact and poorly drilled holes, to model the degradation rate of residual strength. Farley [7] conducted experiments on various composite laminate panels impacted by an aluminum sphere at low velocities. The research used experimental and analytical methods to determine residual strength of composite laminates after sustaining impact damage. In more recent years, Saether [8] developed and utilized a computer program, RESTRAN (RESidual STrength ANalysis), to predict residual strength of composite laminates after impact damage, based on known material and structural failure modes. Koo et al. evaluated the residual tensile strength and fatigue characteristics of carbon fiber reinforced polymer (CFRP) composites after impact damage [9]. By conducting tensile experiments after impact loading, Koo concluded that residual strength decreases as impact energy increases, beyond a determined threshold. Koo used a curve-fit equation to create a prediction model for residual tensile strength after impact.

Damage due to fatigue loading also affects the residual strength of composite materials, as previous studies have demonstrated. Ruiz [10] conducted research on crossply metal matrix composites (MMC), tested under strain and load control, at an

elevated temperature (427°C). This research identified a direct relationship between residual strength and existing matrix damage in the MMC. The study also identified a relationship between the strength degradation rate and ply orientation.

Work by Arora et al. [11] utilized full-scale blast experiments to determine the compressive residual strength of CFRP and glass fiber reinforced polymer (GFRP) sandwich materials. The residual strength tests were performed on cut sections of the original sandwich structure. Arora compared the residual strength to the number of cracks and percentage of debonded area in each blasted sandwich structure. Arora shows that a higher number of recorded cracks in a blasted composite sandwich structure causes a decrease in its compressive residual strength.

Although the residual strength of composite materials has been studied previously, this research is unique because it focuses on the residual strength after blast loading. While similar research has been done on composite sandwich structures [11], this research studies solid laminate composite materials. Experimental techniques are used to induce blast damage, quantify damage, and measure residual strength. Furthermore, this work is unique because of the specimen material and geometry, test environment, and method of damage evaluation. While the work by Arora et al. [11] conducted full-scale blast experiments, this study uses controlled shock loading via a shock tube, creating a more fundamental study to understand the basic physics of residual strength as a result of blast damage. The approach is also unique because it uses non-destructive imaging technologies—Terahertz (THz) and Flash Infrared Thermography (FIRT)—to evaluate the damage through the thickness of a composite laminate.

The following sections describe the methods used to characterize, shock load, image, and evaluate the strength and damage of Cyply 1002 composite laminate panels. The thesis also develops an analytical relationship to predict the compressive residual strength, σ_R , of a Cyply 1002 laminate panel, using a combined damage parameter, d_c , calculated using THz and FIRT damage data.

MATERIAL STUDIED

The research evaluated the compressive residual strength of laminate panels of Cyply 1002, after exposure to controlled blast loading. Cyply 1002 is a cured epoxy composite material reinforced with type-E continuous filament fiberglass, manufactured by Cytac Solvay Group of Winona, MN. Water-jet technology was used to cut the Cyply 1002 into 304.8 x 304.8 mm (12 x 12 in) panels. A thickness of 1.52 mm (0.06 in) was selected to ensure effective shock blast experiments and non-destructive imaging.

The panels were manufactured with two different fiber orientations—crossply and isotropic—each offering different physical properties. The crossply layup sequence is $[0^\circ/90^\circ/0^\circ/0^\circ/90^\circ/0^\circ]$ and the isotropic layup sequence is $[-30^\circ/30^\circ/90^\circ/-60^\circ/60^\circ/90^\circ]$. The material properties, determined through quasi-static experiments, are shown in the “Material Characterization” section of this document.

RESEARCH OUTLINE

General Overview

The research begins with baseline material characterization of Cyply 1002 specimens, per ASTM standards for tension, flexure, and compression [12-14]. Following material characterization, the undamaged 304.8 mm x 304.8 mm x 1.52 mm (12 in x 12 in x 0.06 in) Cyply panels were imaged using non-destructive, through-thickness imaging techniques to form a baseline prior to blast damage. Shock tube blast experiments were conducted on the panels to induce non-catastrophic damage. Following the blast experiments, the panels were imaged again in their damaged state, allowing for quantification of damage. Compressive residual strength experiments were then conducted on the damaged panels. Using data gained from the imaging and residual strength tests, a relationship between damage and compressive residual strength was developed. A flow chart of the research approach is shown in Figure 1.

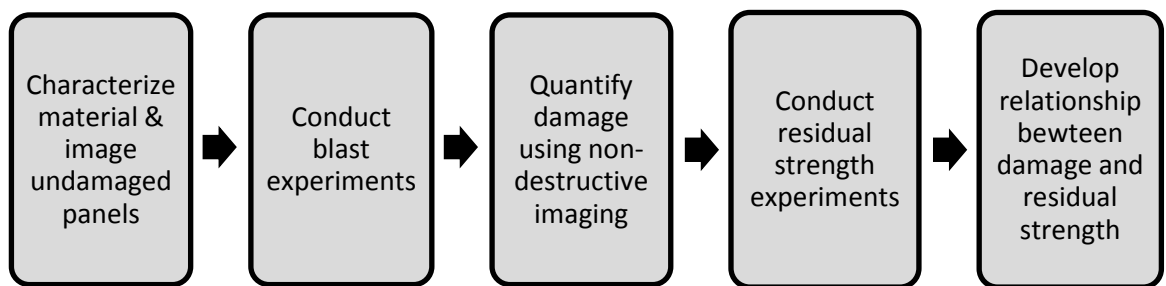


Figure 1. Research approach

The research required the use of several facilities, including the shock tube and high speed photography with three dimensional (3D) Digital Image Correlation (DIC)

at the University of Rhode Island (URI), and non-destructive imaging technologies at the Naval Undersea Warfare Center Division, Newport (NUWC DIVNPT).

Shock Tube

The blast experiments were conducted using the shock tube facility at URI's Dynamic Photomechanics Laboratory (DPML). The shock tube, depicted in Figures 2 and 3, can be used to obtain controlled shock loading up to 7.5 MPa (1,100 psi), representative of an air blast. The shock tube has an overall length of 8 m (26.2 ft) consisting of three rigid cylindrical sections: the high-pressure driver section, low-pressure driven section, and muzzle. The driver and driven sections are separated by a diaphragm [15].

Helium gas is used to pressurize the driver section, creating a pressure differential across the diaphragm. Once a critical pressure is reached, the diaphragm bursts. The high pressure differential creates a shock wave, which travels down the driven section to the muzzle, where it imparts a planar shock load on the specimen [16]. Mylar sheets are used as the diaphragm; the number of Mylar sheets, with a known thickness, controls the pressure of the incident shock wave. Three piezoelectric pressure transducers are mounted in the muzzle end of the shock tube to obtain pressure data throughout the shock event. Further details of the shock tube experiments are provided in the "Shock Loading Experiments" section of this document.

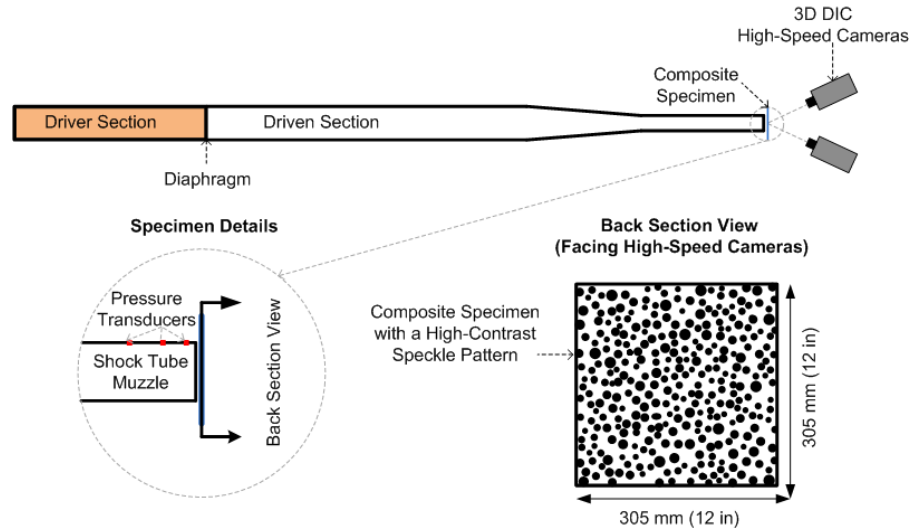


Figure 2. Diagram of the shock tube facility

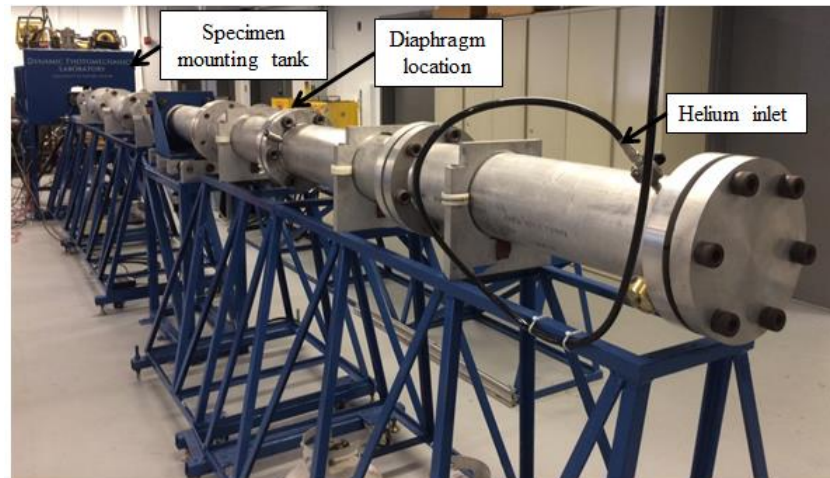


Figure 3. Shock tube facility in the Dynamic Photomechanics Laboratory

High Speed Photography and Digital Image Correlation (DIC)

DIC is used to capture the transient response of the laminate panels during the blast experiments and the quasi-static material characterization tests. DIC is a non-contact technique that captures the full-field displacement response of a specimen.

Two-dimensional (2D) DIC was used for material characterization, capturing in-plane displacements and strains throughout the quasi-static experiments. To use this

technique, the front face of each specimen was painted with a fine high-contrast speckle pattern, which was photographed by one Prosilica GC2450 camera and subsequently analyzed with Vic-2D 6 software (Correlated Solutions Inc., Columbia, SC). DIC is a well-known non-contact method of acquiring full-field displacement data [17].

3D DIC was used for the blast and residual strength experiments. To use this technique, the back surface of the composite specimen was painted with a high-contrast speckle pattern, which was recorded by two Photron FASTCAM SA1.1 high-speed cameras coupled with high-intensity light sources [18], as shown previously in Figure 2. From this recording, it is possible to determine the 3D coordinates of every dot at each point in time. The accompanying image correlation software, or Vic-3D 7 (Correlated Solutions Inc., Columbia, SC), then analyzes these images to provide the full-field displacements, strains, and velocities on the entire back surface of the panel.

Non-destructive Imaging Technologies

Non-destructive through-thickness imaging was conducted on the 304.8 mm x 304.8 mm x 1.52 mm (12 in x 12 in x 0.06 in) panels before and after the blast experiments, as a means of quantifying damage. Two imaging techniques—Terahertz (THz) and Flash Infrared Thermography (FIRT)—are available in the Non-destructive Test and Evaluation Laboratory at NUWCDIVNPT.

The THz system uses a broadband THz-frequency pulse to interrogate the composite panels, returning time-of-flight data for analysis. MATLAB was used to create a 3D map of the internal structure and reveal measurable defects and damage

within the specimen. The FIRT system uses a high-intensity flash to heat the panel surface, which is viewed by an infrared camera. The time-variant heat patterns on the material surface provide information about the defects and damage throughout the thickness of the panel. Both techniques were used to quantify the panel damage, since each offers different capabilities and strengths for damage evaluation. Further details about the THz and FIRT systems are provided in the “Imaging Systems and Damage Quantification” section of this document.

MATERIAL CHARACTERIZATION EXPERIMENTS

Baseline material characterization was conducted to determine material properties of the undamaged crossply and isotropic Cyply 1002 composite laminates. Tension, flexure, and compression experiments were conducted per applicable ASTM standards.

Methods

Each specimen was prepared for DIC by applying a layer of white spray paint, overlaid with a fine mist of black spray paint to create a speckle pattern. For all material characterization experiments, one Prosilica GC2450 camera was used to record images throughout the test. Images were captured at 1 frame per second, with a 50 mm lens, 512 x 512 resolution, and an aperture of 4.2.

Tensile experiments were conducted per ASTM D3039: Standard Test Method for Tensile Properties of Polymer Matrix Composite Materials [12], allowing for the calculation of tensile chord modulus and the ultimate tensile strength. Using waterjet technology at NUWC DIVNPT, five 25.4 mm x 254 mm x 1.52 mm (1 in x 10 in x 0.06 in) specimens were cut from the each of the crossply and isotropic laminates. The front face of each specimen was painted for DIC, and emery cloth tabs were attached using JB Weld adhesive, as shown in Figure 4. The 25.4 mm x 25.4 mm (1 in x 1 in) tabs were attached on the top and bottom of both faces, to prevent premature failure due to slipping.



Figure 4. Tensile specimen with emery cloth tabs, painted for DIC

Tensile load and extension data were collected through the test machine, INSTRON 5585 and the accompanying Merlin software, while strain data was produced through 2D DIC. By combining these vectors in MATLAB, material properties were calculated using Equations 1 and 2:

$$\sigma_{ut} = \frac{P_{max}}{A_t} \quad (1)$$

where σ_{ut} is the ultimate tensile strength, P_{max} is the maximum tensile load applied before failure, and A_t is the cross-sectional area of the tensile specimen, 25.4 mm x 1.52 mm (1 in x 0.06 in);

$$E_t = \frac{\Delta \sigma}{\Delta \varepsilon} \quad (2)$$

where E_t is the tensile chord modulus of elasticity, $\Delta \varepsilon$ is the difference between two strain points, and $\Delta \sigma$ is the difference in applied tensile stress between these strain points.

Four-point-bend experiments were conducted per ASTM D7264: Standard Test Method for Flexural Properties of Polymer Matrix Composite Materials—Procedure B [13], allowing for the calculation of the flexural chord modulus and the ultimate flexural strength. The flexural tests were conducted on the INSTRON 3366, shown in Figure 5. Using waterjet technology at NUWC DIVNPT, five 12.7 mm x 63.5 mm x 1.52 mm (0.5 in x 2.5 in x 0.06 in) specimens were cut from the each of the crossply and isotropic laminates. One side of each specimen was speckled for DIC.

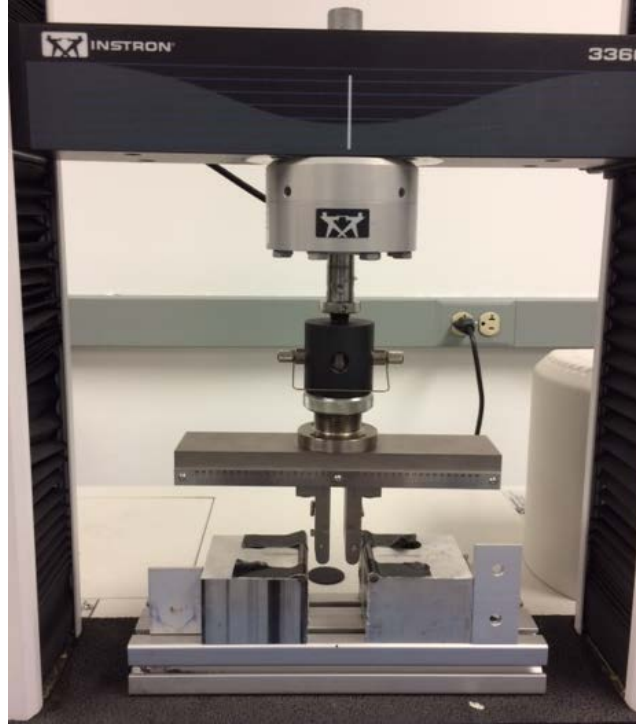


Figure 5. INSTRON 3366 set up for Four-Point-Bend tests

Load and flexural extension data were collected through the INSTRON 3366 and accompanying Merlin software, while through-thickness strain data was produced through 2D DIC. After importing load, extension, and strain data into MATLAB, material properties were calculated using the Equations 3, 4, and 5:

$$\sigma_{uf} = \frac{3P_{max}L}{4bh^2} \quad (3)$$

where σ_{uf} is the ultimate flexural strength in the outer surface of the load span region, P_{max} is the maximum flexural load applied by the INSTRON 3366 prior to failure, L is the support span, b is the width of the specimen, and h is the thickness of the specimen;

$$\varepsilon = \frac{4.36\delta h}{L^2} \quad (4)$$

where ε is the maximum strain at the outer surface, δ is the maximum mid-span deflection, L is the support span, and h is the thickness of the specimen;

$$E_f^{chord} = \frac{\Delta \sigma}{\Delta \varepsilon} \quad (5)$$

where E_f^{chord} is the flexural chord modulus of elasticity, $\Delta \varepsilon$ is the difference between two strain points, and $\Delta \sigma$ is the difference in flexural stress between these strain points.

Compression experiments were conducted per ASTM D3410: Standard Test Method for Compressive Properties of Polymer Matrix Composite Materials with Unsupported Gage Section by Shear Loading [14], allowing for the calculation of the compressive modulus and the ultimate compressive strength. Compression tests were conducted on a fixture designed per ASTM D3410, shown in Figure 6.

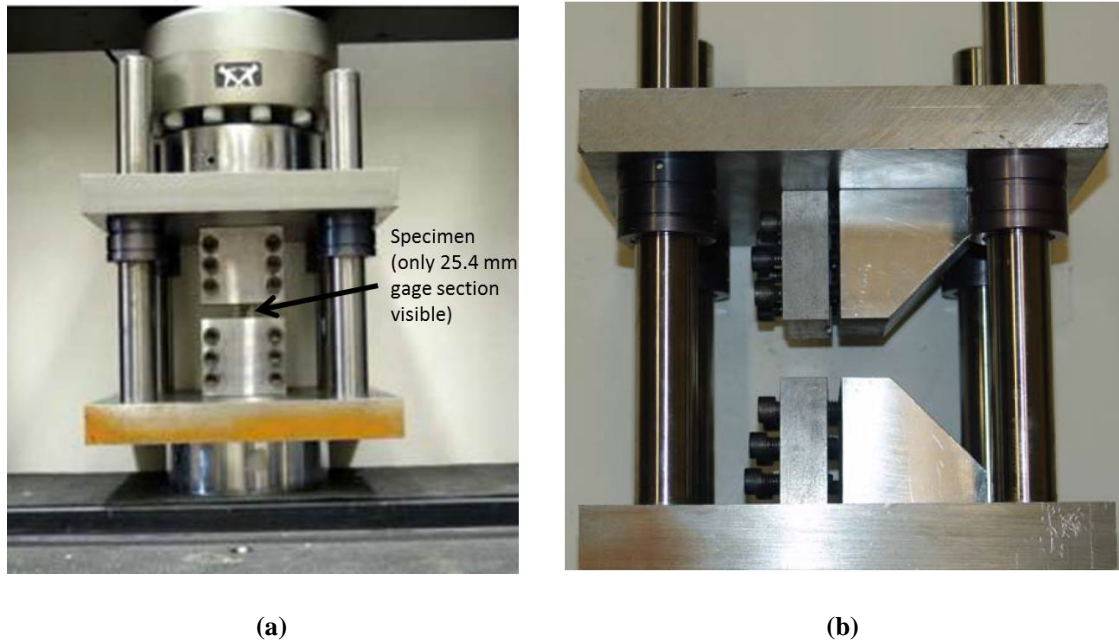


Figure 6. (a) Front view of compression fixture with specimen painted for DIC [3], and (b) side view of compression fixture, showing empty specimen grooves

Using a diamond blade wet saw in the DPML, six 19.05 mm x 152.4 mm x 1.52 mm (0.75 in x 6 in x 0.06 in) specimens were cut from the each of the crossply and isotropic laminates. The front face of each specimen was painted for DIC, and emery cloth tabs were attached using JB Weld adhesive. The 19.05 mm x 63.5 mm (0.75 in x 2.5 in) tabs were attached on the top and bottom of both faces, to prevent premature failure due to slipping in the fixture. This created a 25.4 mm (1 inch) long gage section, in accordance with ASTM D3410.

Compressive load and displacement data were collected through the INSTRON 5585 and accompanying Merlin software, while strain data was produced through 2D DIC. By combining these vectors with MATLAB, material properties were calculated using Equation 6:

$$\sigma_{uc} = \frac{P_{max}}{A_c} \quad (6)$$

where σ_{uc} is the ultimate compressive strength, P_{max} is the maximum compressive load applied before failure, and A_c is the cross-sectional area of the compression specimen, 19.05 mm x 1.52 mm (0.75 in x 0.06 in).

Results

Tension, compression, and flexure tests were conducted on crossply and isotropic Cyply 1002 specimens. For each material test, at least five valid tests were required to calculate accurate material properties. 2D DIC was used to calculate in-plane displacements and strains for each specimen. Figures 7 through 9 shows a specimen after failure for each test type, with the DIC strain contour shown.

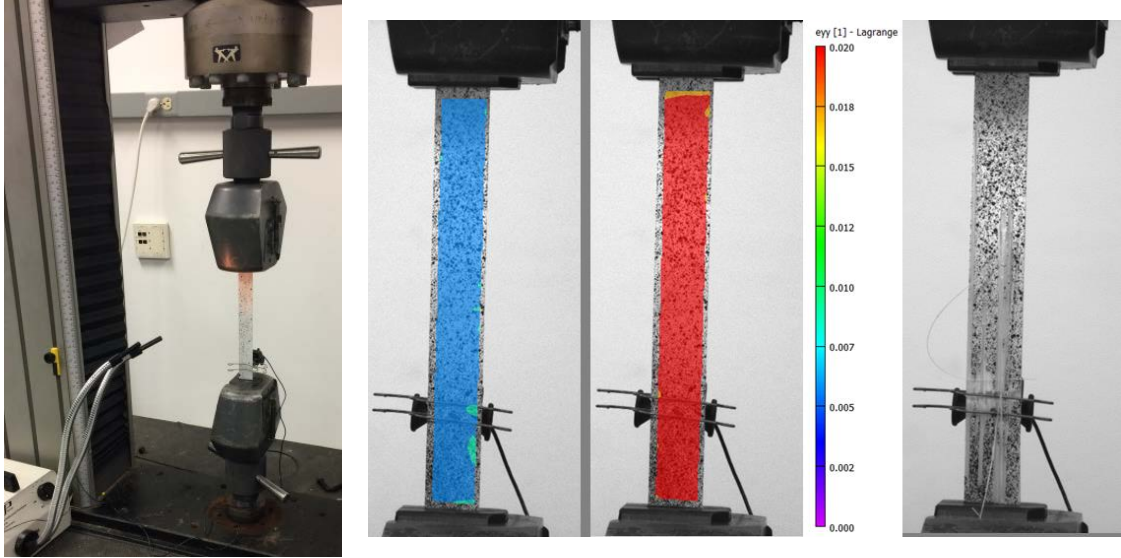


Figure 7. Tensile Test Setup (left) and DIC Strain Contour of Specimen Failure (right)

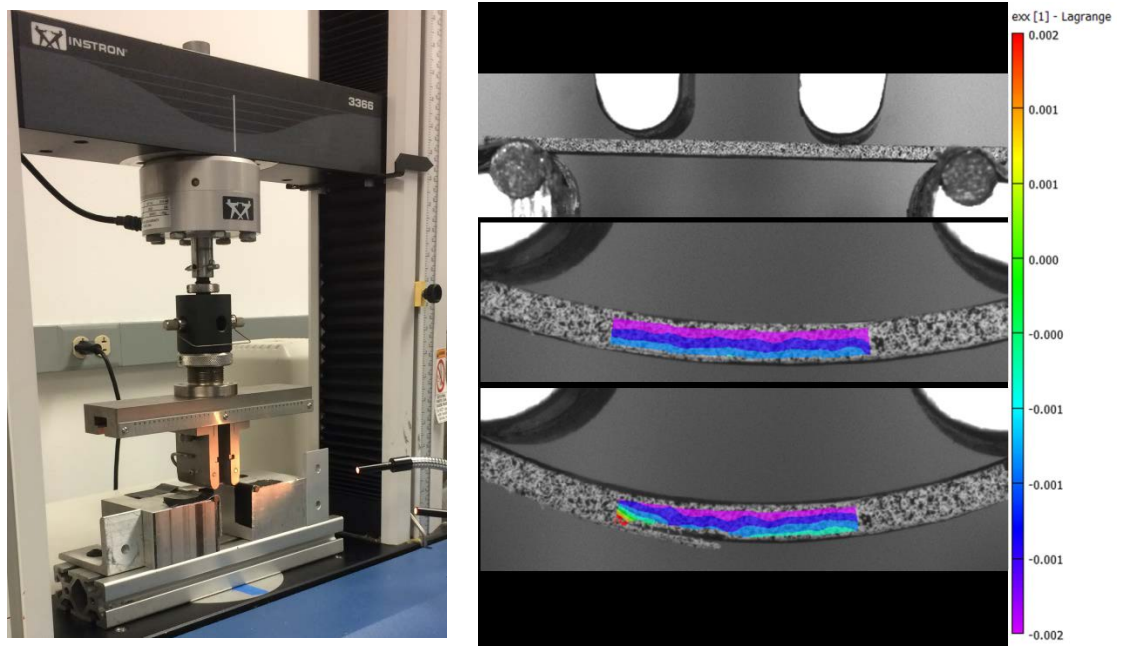


Figure 8. Flexure test setup (left) and DIC strain contour of specimen failure (right)

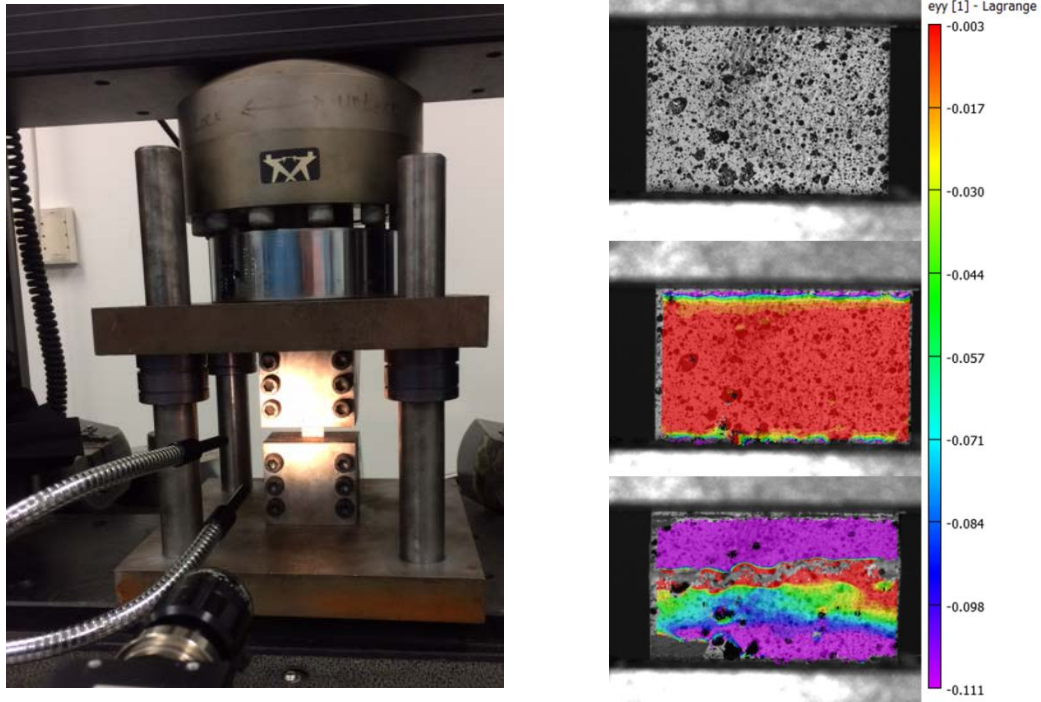


Figure 9. Compression test setup (left) and DIC strain contour of specimen failure (right)

Material properties were calculated using data from the INSTRON machines, DIC, and MATLAB. Table 1 shows the results of the material characterization experiments for crossply and isotropic Cyply 1002.

Table 1. Mechanical properties of crossply and isotropic Cyply 1002

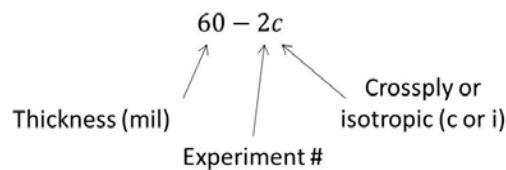
	Crossply [0°/90°/0°/0°/90°/0°]	Isotropic [-30°/30°/90°/-60°/60°/90°]
Tensile strength, MPa (psi x 10³)	330 (47.9)	283 (41.0)
Tensile strain (%)	1.7	2.3
Tensile modulus, GPa (psi x 10⁶)	24.6 (3.56)	14.8 (2.15)
Flexural strength, MPa (psi x 10³)	728 (106)	495 (71.8)
Flexural strain (%)	2.6	2.8
Flexural chord modulus, GPa (psi x 10³)	47.4 (6.87)	20.7 (3.00)
Compressive strength, MPa (psi x 10³)	379 (55.0)	240 (34.8)

SHOCK LOADING EXPERIMENTS

Blast experiments were conducted using URI's shock tube facility, previously shown in Figure 2, to induce non-catastrophic shock damage on the Cyply 1002 laminate panels.

Methods

Nine experiments were conducted on the shock tube to expose five crossply panels and four isotropic panels to controlled air blast loading. Each panel was labeled with the following naming convention:



Each 304.8 x 304.8 x 1.52 mm (12 in x 12 in x 0.06 in) panel was mounted at the muzzle end of the shock tube and subjected to a planar shock wave with an average peak incident pressure of 0.9 MPa (130 psi). The composite panel was mounted on a square fixture, simply supported with two elastic bands as shown in Figure 10. The simply supported boundary condition allows the panel to move freely and avoids the risk of boundary crushing or unintended slipping that can occur with fully clamped boundary conditions.

The shock tube was configured with a 38.1 mm (1.5 inch) inner diameter muzzle. The center of the panel was aligned with the center of the shock tube muzzle. Figure 10 also shows three piezoelectric pressure sensors (PCB 138A05, PCB Piezotronics,

Inc., Depew, NY), which were used to record high-frequency pressure data during the shock event. The pressure transducer furthest from the specimen, with a sensitivity of 5 mV/psi, triggered the oscilloscope and the high speed cameras. The two pressure transducers closest to the specimen have a sensitivity of 1 mV/psi and were used to capture the reflected pressure of the shock wave, which is the actual pressure seen by the composite panel. The amplified outputs of these sensors are monitored by Tektronix DPO 3034 Digital Phosphor oscilloscope, at a frequency of 1 MHz for 10,000 samples.

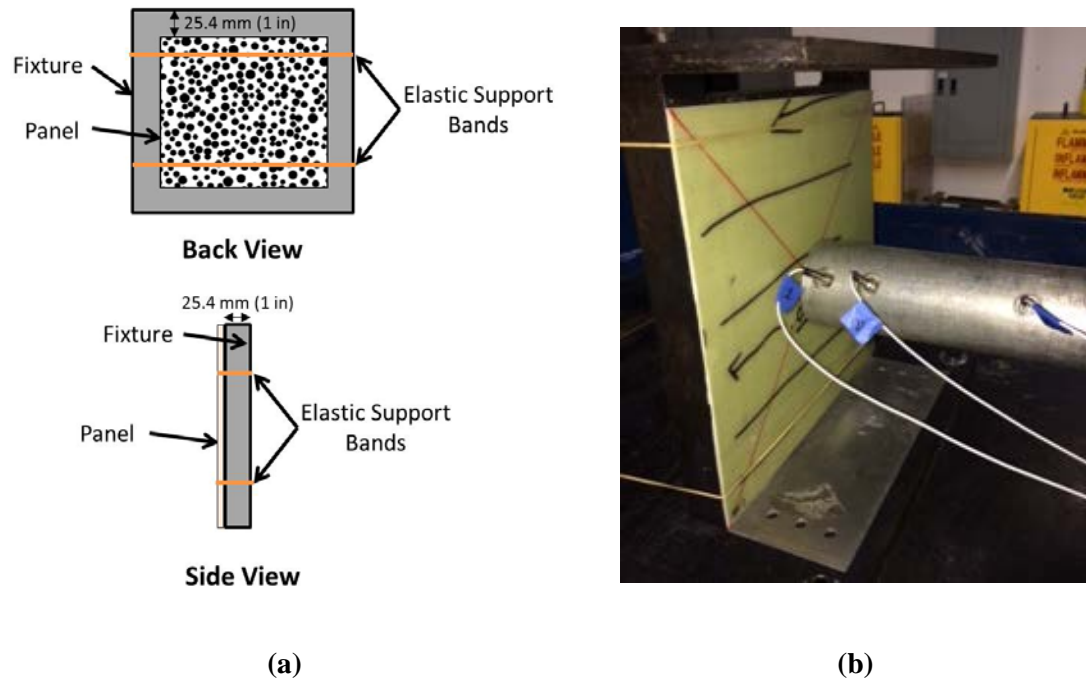


Figure 10. (a) Schematic of mounting fixture and (b) composite panel mounted in front of shock tube muzzle

Each panel was prepared for DIC by applying a layer of white spray paint, overlaid with a random black speckle pattern. Two Photron FASTCAM SA1.1 high speed cameras were used to record images throughout the shock event. Images were captured at 20,000 frames per second, with a 28 mm lens, 512 x 512 resolution, and an aperture of 8. The high speed cameras were set up behind the specimen mounting tank

to record the blast event through two Lexan polycarbonate windows. The cameras and DIC system were calibrated prior to each set of shock tube experiments to ensure data accuracy, as shown in Figure 11.

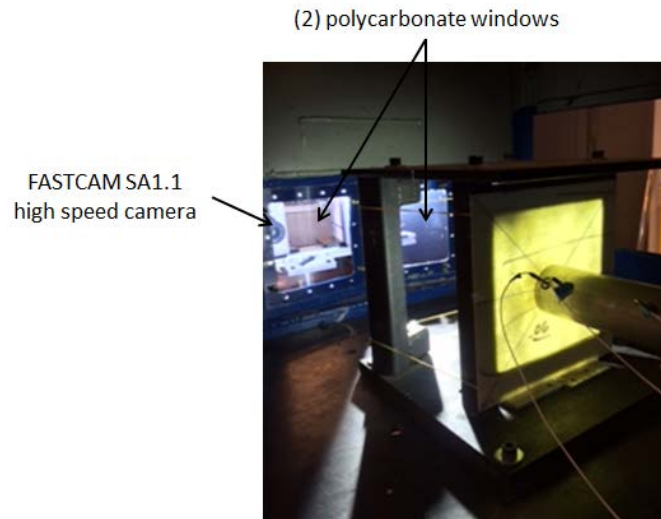


Figure 11. Arrangement of panel and Lexan windows for high speed photography

Prior to the nine shock tube experiments, several trial experiments were conducted to determine which incident pressure—controlled by the diaphragm thickness—would induce a desired amount of damage in the panels. In order to test a range of incident shock pressures, the thickness of the shock tube diaphragm was adjusted by adding or removing individual 0.254 mm (10 mil) Mylar sheets. The trial experiments showed that a 0.508 mm (20 mil) diaphragm produced a significant, yet non-catastrophic, amount of damage.

Results

Pressure and 3D DIC data were collected for five crossply panels and four isotropic panels, as shown in Table 2. The incident pressures were consistent with a maximum difference of only 13%, demonstrating that a valid test series was

conducted. The reflected pressure pulse represents the true pressure experienced by each panel, as the shock wave reflects against the specimen and back into the tube with a larger pressure magnitude [15]. Figure 12 shows the pressure profiles for each experiment; the pressure profiles align well for all nine experiments, showing an incident pressure of 0.91 ± 0.04 MPa (132 ± 5.8 psi) and a reflected pressure of 3.23 ± 0.20 MPa (468 ± 30 psi), for all panels excluding 60-1c since it was set up with a diaphragm twice as thick as the other panels. The thicker diaphragm caused a much higher shock pressure and induced significantly more damage.

Table 2. Blast pressures and out-of-plane displacements for shock tube experiments

Panel	Diaphragm Thickness	Incident Pressure	Reflected Pressure	Maximum Out-of-Plane Displacement	Preliminary Observed Damage
60-1c	1.016 mm (40 mil)	1.54 MPa (224 psi)	5.3 MPa (772 psi)	83 mm (3.27 in)	Large through-thickness crack, fiber breakage, and delamination on most of panel.
60-2c	0.508 mm (20 mil)	0.87 MPa (126 psi)	3.2 MPa (468 psi)	62 mm (2.44 in)	Delamination and fiber breakage near center
60-5c	0.508 mm (20 mil)	0.91 MPa (132 psi)	3.6 MPa (516 psi)	62 mm (2.46 in)	Fiber breakage and delamination in left and right top quadrants
60-7c	0.508 mm (20 mil)	0.93 MPa (135 psi)	3.2 MPa (457 psi)	60 mm (2.36 in)	Crack and delamination on right
60-9c	0.508 mm (20 mil)	0.88 MPa (128 psi)	3.2 MPa (459 psi)	61 mm (2.40 in)	Crack and delamination on right side
60-1i	0.508 mm (20 mil)	0.94 MPa (136 psi)	3.7 MPa (540 psi)	79 mm (3.11 in)	Large crack in left center, delamination and fiber breakage on left side and around edges.
60-2i	0.508 mm (20 mil)	0.85 MPa (123 psi)	3.8 MPa (548 psi)	75 mm (2.95 in)	Large crack near left center and edge, and panel bending
60-4i	0.508 mm (20 mil)	0.94 MPa (136 psi)	3.1 MPa (454 psi)	74 mm (2.91 in)	Crack near center and diagonal delaminated region across left, right and, center
60-7i	0.508 mm (20 mil)	0.94MPa (136 psi)	3.0 MPa (437 psi)	63 mm (2.48 in)	Crack near center and diagonal delaminated region across left, right and, center

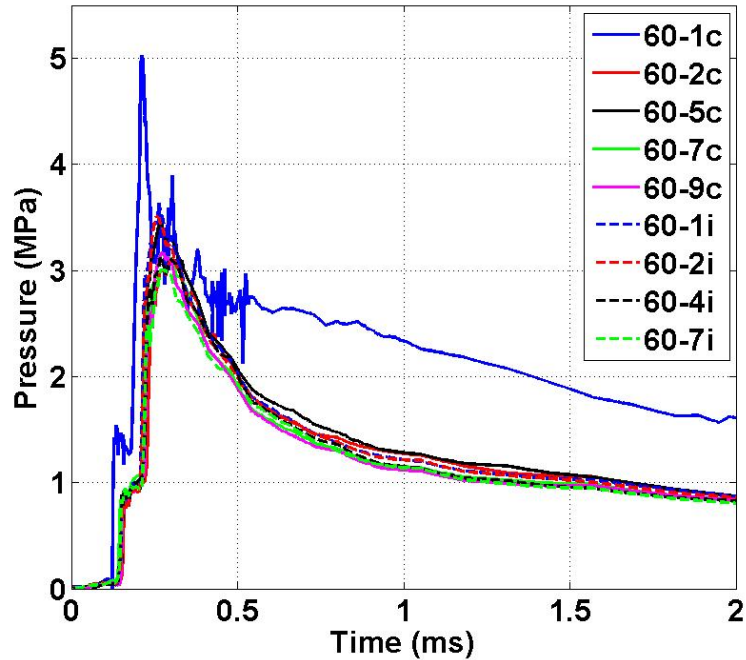


Figure 12. Pressure profiles from shock tube experiments—crossply and isotropic panels

Although each panel was carefully set up with the same conditions and was exposed to the same pressures (with the exception of 60-1c), a variety of damage was seen across the 9 panels. This variety of damage is important for the development of a relationship between compressive residual strength and damage.

To better understand the damage incurred by each panel, a thorough analysis of each panel was conducted using the DIC data and the accompanying software, VIC-3D. This software takes the images captured by the high speed cameras and calculates full-field displacements and strains. Figure 13 shows three images of panel 60-2i; these images were captured before, during, and after the blast load. Figure 14 shows the maximum out-of-plane displacement of panel 60-2i during the shock experiment, computed by the VIC-3D analysis. Similar images for all nine panels are provided in

Appendix A. The maximum center-point displacement for each panel is provided in Table 2.

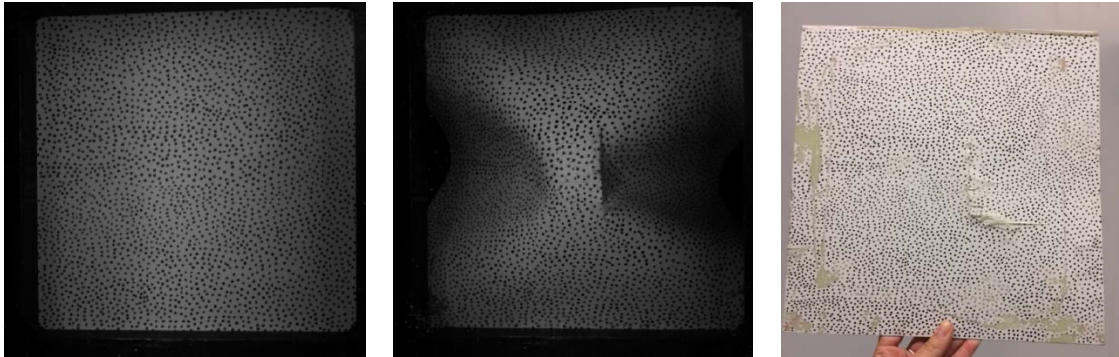


Figure 13. Panel 60-2i before (left), during (middle), and after (right) blast load

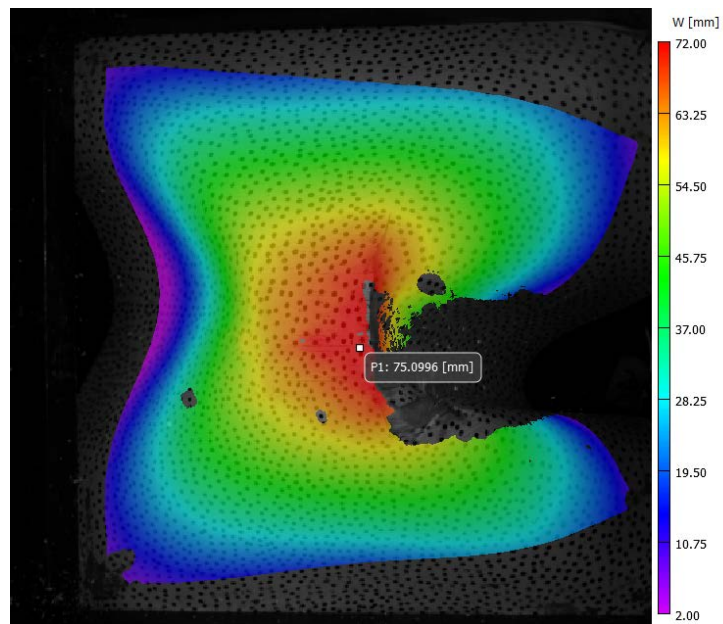


Figure 14. Panel 60-2i maximum out-of-plane displacement (W) during blast

Following each blast experiment, a preliminary visual inspection of the damaged panel was conducted, as noted in Table 2. Figure 15 shows the preliminary damage observed for panel 60-2i; similar photographs are provided for all panels in Appendix A.

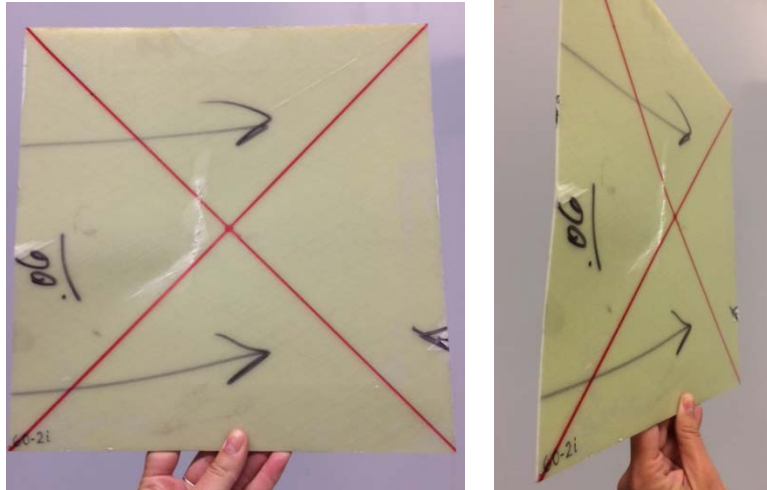


Figure 15. Damage in panel 60-2i after blast loading—front face (left) and side (right)

Nearly all panels suffered some cracking and delamination, while remaining structurally intact, as described in Table 2. High speed photography shows that the panels deformed outward during the blast, but returned to a relatively flat shape after the blast. Panel 60-1c, which was blasted with nearly twice as much pressure, had significantly more through-cracking and delamination than the other eight panels, as expected. A thorough evaluation of damage was later conducted using THz and FIRT imaging technologies, as presented later in this document.

IMAGING SYSTEMS AND DAMAGE QUANTIFICATION

The Flash Infrared Thermography (FIRT) and the Terahertz (THz) imaging system are non-destructive evaluation technologies available through NUWCDIVNPT, which can provide through-thickness images of the pre- and post-shock composite panels. This technology allows for the identification of internal defects, delamination, and provides a method for quantifying such damage. Both techniques were used to quantify panel damage, since each offers different capabilities and strengths for damage evaluation.

After imaging the nine damaged 304.8 mm x 304.8 mm (12 in x 12 in) panels, each panel was cut into three subpanels, allowing for residual strength testing, as well as creating an increased number of data points for relationship development. The FIRT and THz data were used to quantify subpanel damage in terms of the following five damage quantities: total length of delaminated edges, total area of delaminated surfaces—internal and external, total volume of delaminated regions, total length of cracks, and total surface area of cracks.

Methods: FIRT Imaging

FIRT imaging was conducted on the front and back faces of all panels before and after the shock tube experiments, creating a baseline for the panels' pre- and post-shock conditions.

The FIRT system, shown in Figure 16, uses two bright bulbs to strobe the composite panel with a high-intensity flash. The two bulbs are charged by capacitors;

when the capacitors are discharged, the bulbs provide a bright rapid flash, immediately heating the surface of the panel. After the flash, the heat diffuses into the thickness of the panel. Obstructions in the panel—such as cracks, delamination, or foreign objects—cause differences in the heat diffusion and create time-variant heat patterns on the surface, which are recorded by an infrared camera. The transient thermal data is sent to Virtuoso software, which provides a graphic user interface to analyze and post-process the data.

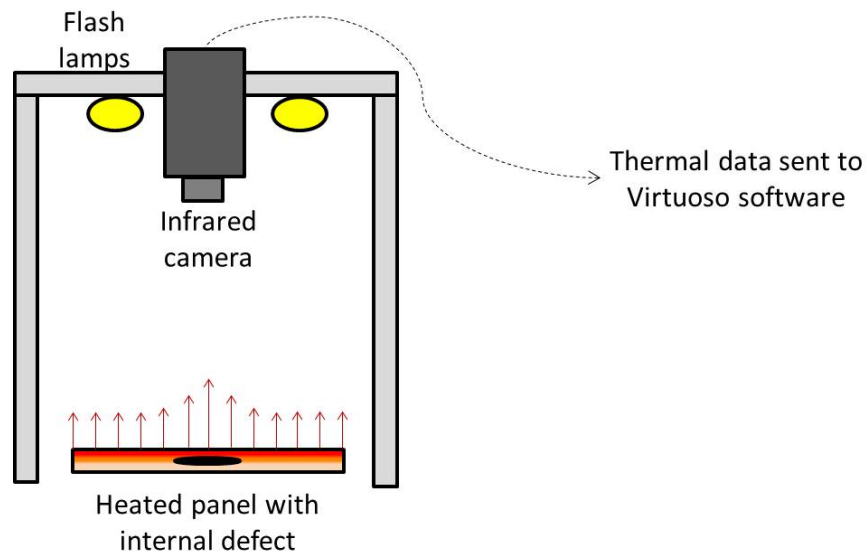


Figure 16. FIRT imaging of damaged composite panel

The transient thermal data provides information about the defects and damage throughout the thickness of the panel. For the 1.52 mm (0.06 in) thick Cyply panels, the heat conducts through the thickness of the composite panel in approximately 2 seconds. The data was processed with two different Virtuoso filters:

- *Thermal Signature Reconstruction (TSR)*: Color map represents the surface temperature which indicates a cumulative response.

- *First Derivative (1D)*: Color map represents the instantaneous rate of change (rate of heating or cooling) of the surface temperature. This shows how quickly heat diffuses through the panel, which varies in damaged regions.

Methods: THz Imaging

THz imaging was conducted on undamaged panels prior to the shock tube experiments, with a resolution of 1 mm². All damaged panels were scanned again by the THz system after the shock tube experiments, with a higher resolution of 0.25 mm². Each THz scan of a 304.8 mm x 304.8 mm (12 in x 12 in) panel requires approximately 50 minutes.

Terahertz imaging uses electromagnetic waves with frequencies between 0.1-10 THz; this frequency range lies between microwave and infrared. THz imaging is biologically safe, providing an advantage for many applications where x-ray computed tomography (CT) may otherwise be required for internal imaging. THz imaging is suitable for the composite material used in this research, Cyply 1002, and also ceramics, epoxies, urethanes, and some rubbers. THz cannot penetrate metal or water.

The THz system, shown in Figure 17, uses time-of-flight data to detect voids, delamination, ply surfaces, and material non-uniformities in Cyply 1002. The THz transmitter and receiver are mounted on a positioning rail, which moves the scanner along the x- and y-axis of the specimen in fixed increments, depending on the desired resolution of the image.

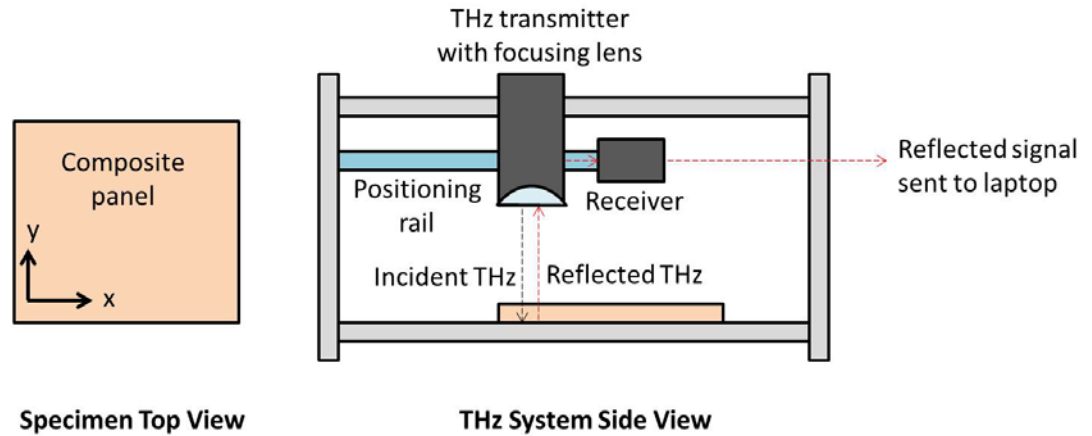


Figure 17. THz system scanning composite panel

As the incident signal reaches a material interface, ply surface, or defect, a fraction of the wave will transmit through, reflect or scatter, with each wave behavior affecting the time-of-flight, measured in picoseconds. Figure 18 demonstrates the path of a THz wave through an undamaged specimen versus a cracked specimen.

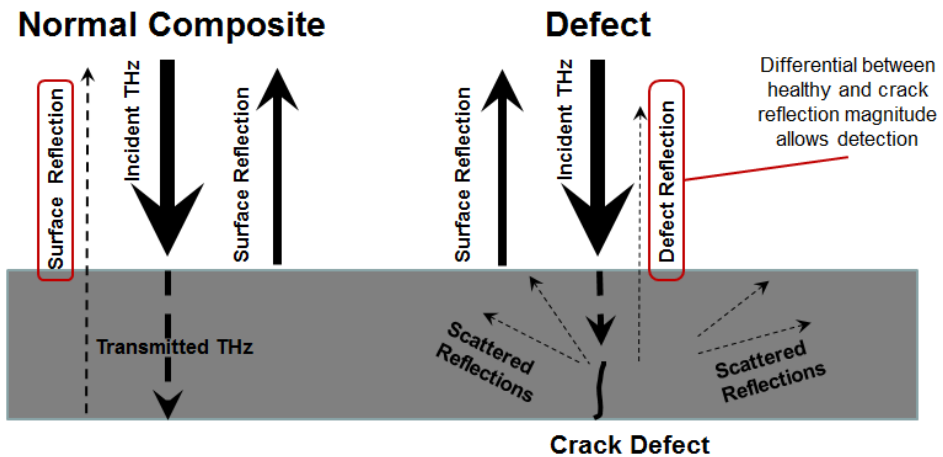


Figure 18. Behavior of THz waves through normal and defected composite material [19]

The pulse time-of-flight data is analyzed by NUWCDIVNPT's in-house MATLAB code to create a 3D map of the panel's internal structure, revealing measurable defects and damage. As shown in Figure 19, data can be visualized and post-processed as a

signal intensity map (x-y plane), depth scan of a row (x-z plane), or depth scan of a column (y-z plane).

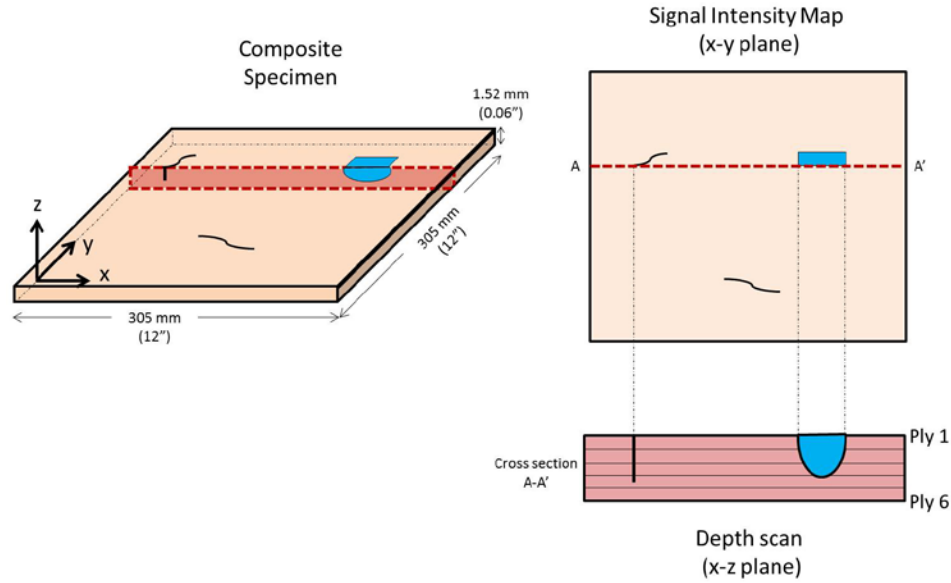


Figure 19. (a) Representation of a damaged composite panel, and THz post-processing image types: (b) signal intensity map of x-y plane and (c) depth scan in the x-z plane

The time-of-flight signal is used with the material's refractive index and the speed of light to calculate the actual distance between surfaces and defects inside each panel. Using the known thickness between the front and back surfaces of the panel, Snell's Law was used to calculate the refractive index, n , of the Cyply 1002 glass fiber/epoxy, as shown in Equation 7:

$$n = c \frac{(t_2 - t_1)}{2h} \quad (7)$$

$$n = \frac{(3 * 10^8 \text{ m/s})(1028 - 775) * 10^{-13} \text{ s}}{2 * (0.001524 \text{ m})}$$

$$n = 2.49$$

where c is the speed of light (m/s), h is the thickness of the panel (m), and t_1 and t_2 are signal return times (s) from the front and back surfaces of the panel, respectively. With

the known refractive index and the time-of-flight signal available at each pixel, the physical size, s , of any defect can be determined using Equation 8:

$$s = \frac{c * (t_2 - t_1)}{2n} \quad (8)$$

Using the depth scans at rows and columns as shown in Figure 19c, this equation can be used to calculate length, width, and depth of an internal defect.

Methods: Damage Quantification

After each damaged 304.8 mm x 304.8 mm (12 in x 12 in) panel was imaged using FIRT and THz technology, each panel was cut into three 101.6 mm x 152.4 mm (4 in x 6 in) subpanels, as shown in Figure 20. This allows for residual strength testing per ASTM D7137 [20], and provides an increased number of data points for relationship development.

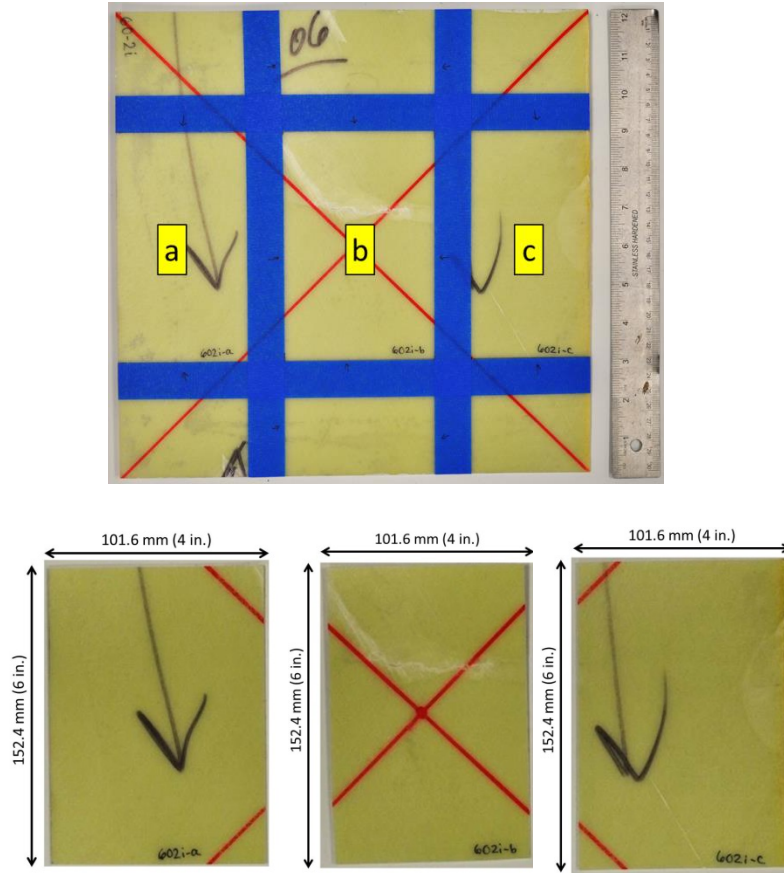


Figure 20. Panel 60-2i (top) cut into three 101.6 x 152.4 mm subpanels (bottom)

Visual inspection with calipers, in conjunction with the FIRT and THz data was used to quantify subpanel damage in terms of the following five damage quantities, d_i :

- d_1 : Total length of delaminated edges (mm)
- d_2 : Total area of delaminated surfaces—internal and external (mm²)
- d_3 : Total volume of delaminated regions (mm³)
- d_4 : Total length of cracks (mm)
- d_5 : Total surface area of cracks (mm²)

Results

After each panel was imaged on the FIRT and THz systems, the data was analyzed to quantify the damage in each subpanel, in terms of the five damage parameters. Each imaging system satisfied a unique purpose while analyzing the data; the FIRT system provided a fast method to identify the presence of damage. Once identified in the FIRT images, damage could be quantified using the THz system's signal intensity maps and depth scans at affected pixel rows and columns.

Figure 21 shows the FIRT thermal signature reconstruction (TSR) image of panel 60-7i, at 0.708 seconds after the flash. In TSR images, blue indicates a cooler temperature and yellow indicates a warmer temperature. The TSR for 60-7i shows two major cracks (Figure 21). Stemming from each major crack, the TSR shows a yellow/pink diagonal strip where the top ply has peeled off, leaving a rough surface with exposed fibers. Additionally, the TSR shows pink regions that represent internal delamination near the cracks. The speckle pattern on the back face is also visible, indicating that the heat has diffused through the thickness of the panel.

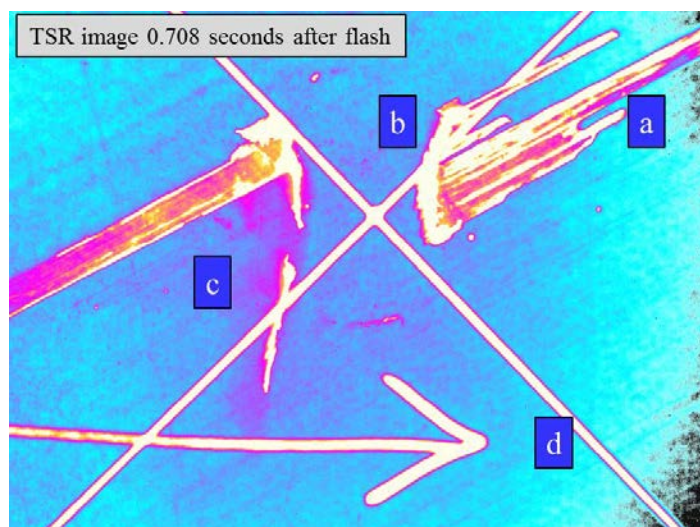


Figure 21. FIRT TSR image of panel 60-7i showing: a) orientation of fibers and ply 1 removal, b) major cracks, c) internal delamination, and d) back face speckle pattern

Once the presence of damage has been established using the FIRT technology, the THz data can be used to further explore the damage and quantify the exact length, width, and depth of any defect. The left side of Figure 22 shows a THz signal intensity map of the damaged area of panel 60-7i, taken with 0.25 mm² resolution and a scanned area of 88 mm x 120 mm (3.5 in x 4.7 in). The right side of Figure 22 shows three depth scans, taken at pixel rows with a variety of damage. Each depth scan shows all six plies that make up the Cyply 1002 composite panels. The depth scan through row 357 shows two through-thickness cracks, as well as internal delamination and peeling of the top ply. Note that the aspect ratio of the depth scans is adjusted to be able to see damage. Knowing that the panel is 1.52 mm thick (0.06 in), the depth of a crack can be measured directly from the depth scan. Additionally, knowing the scanning area—for Figure 22, 88 mm x 120 mm—the width of a defect can be calculated directly from a row depth scan, while the length of defect must be determined from a column depth scan.

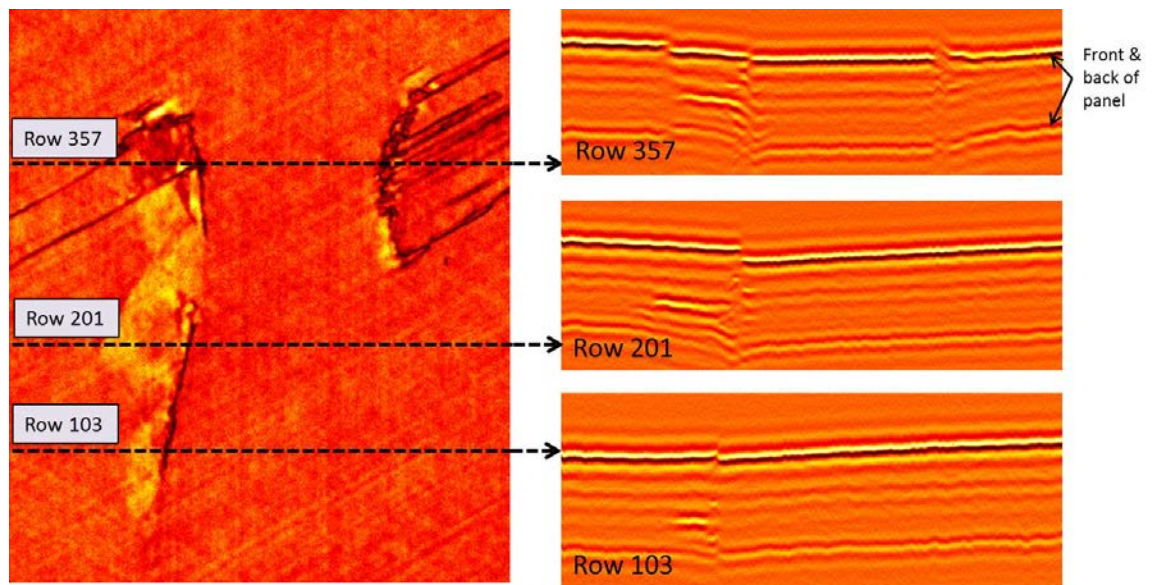


Figure 22. Panel 60-7i THz images—signal intensity map (left) and three depth scans (right) showing depth and location of cracks and delamination

Figure 23 examines the depth scan at row 201 more closely, providing dimensions of the internal defects. The signal intensity map (top) and depth scan (bottom) are aligned so the damage in the x-y plane can be visualized simultaneously with the damage in the z-plane.

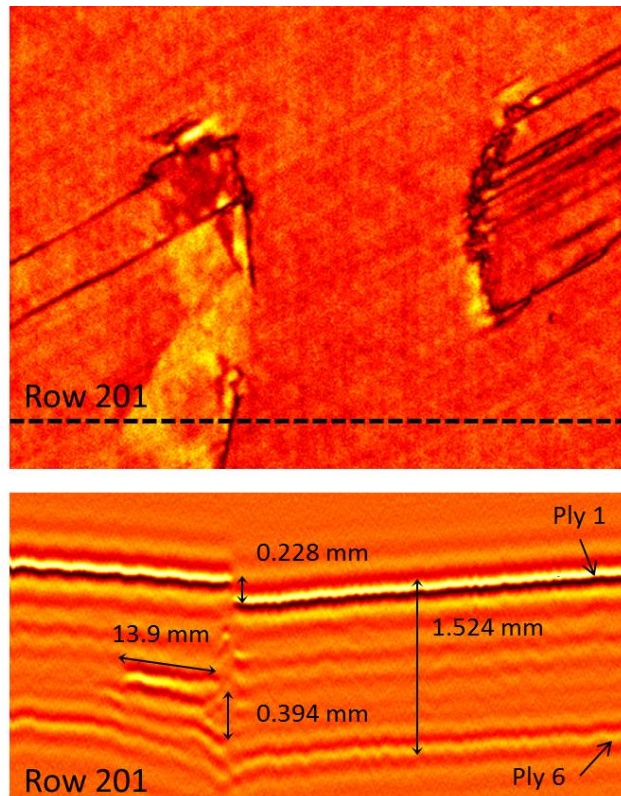


Figure 23. Panel 60-7i damage quantification using a THz row depth scan (bottom) aligned with a signal intensity map (top)

By repeating this depth scan analysis at all damage locations, the damage quantities were obtained for all nine panels—and therefore, all 27 subpanels. The FIRT and THz images for all panels are shown in Appendix B. Additional information can be obtained through a variety of other THz image types, such as surface contours and internal surface maps, shown in Figure 24. The surface contour map uses color gradient to indicate a change in height of the surface, indicating a bent surface. If the

panel is perfectly flat, the surface contour map will show one color. The internal surface map uses a frequency windowing technique to isolate internal surfaces. This technique is helpful for identifying the shape of internal delamination.

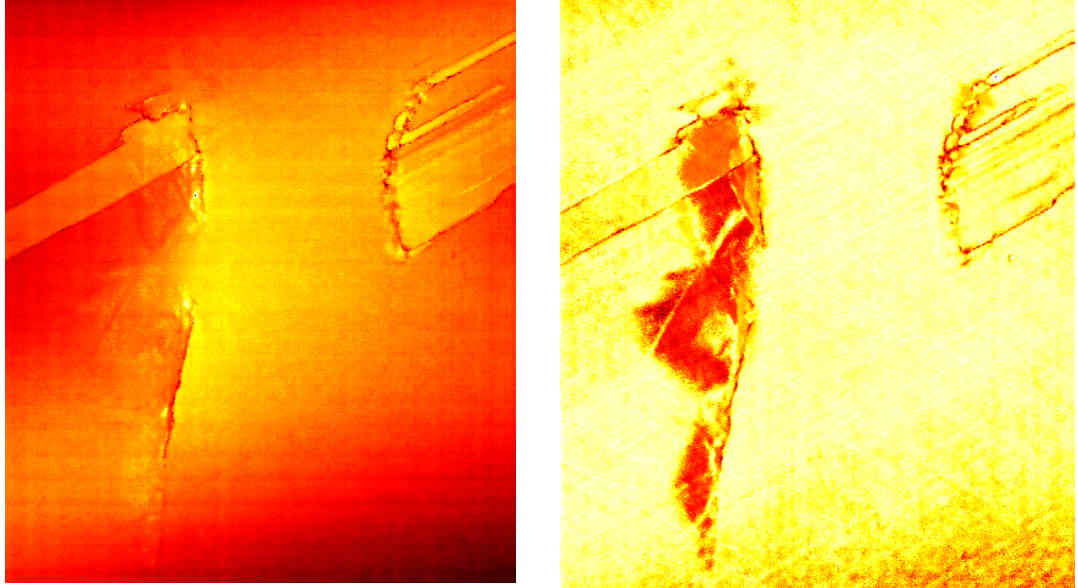


Figure 24. THz images of center region of 60-7i :surface contour map (left) indicating slope of the panel surface, and internal surface map (right) showing delamination at the internal surfaces only

While analyzing each panel, the following damage quantities, d_i , were recorded:

- d_1 : Total length of delaminated edges (mm). This quantity was measured using calipers and represents the sum of all delaminated edge lengths.
- d_2 : Total area of delaminated surfaces—internal and external (mm^2). This quantity was measured using THz depth scans at delaminated rows and columns and represents the sum of all delaminates surface areas.
- d_3 : Total volume of delaminated regions (mm^3). This quantity multiplies each delaminated area (determined while calculating d_2) by the depth of that specific delaminated region, which is identified through THz depth scans and represents the sum of all delaminated region volumes.

- d_4 : Total length of cracks (mm). This quantity was measured with calipers for surface cracks, and THz depth scans for internal cracks and represents the sum of all crack lengths.
- d_5 : Total surface area of cracks (mm^2). This quantity uses the length of a crack (determined while calculating d_4) and multiplies it by the depth of the crack, which is determined through THz depth scans and represents the sum of all crack surface areas.

The damage summary for all subpanels is shown in Table 3. Recall that panel 60-1c was shocked with a much stronger pressure wave as shown previously in Table 2; therefore, significantly higher damage was reported. Of the 27 subpanels evaluated, 10 did not have any reported damage.

Table 3. Damage quantities for all subpanels determined through THz and FIRT

Subpanel	d₁: Total Length of Delaminated Edges (mm)	d₂: Total Area of Delaminated Surfaces (mm²)	d₃: Volume of Delaminated Regions (mm³)	d₄: Total Length of Cracks (mm)	d₅: Total Surface Area of Cracks (mm²)
60-1c (a)	203.1	5,072	1,943	29.92	41.52
60-1c (b)	187.7	12,140	10,300	237.0	252.1
60-1c (c)	105.7	2,272	928.4	26.31	29.73
60-1i (a)	19.13	55.44	23.38	0.000	0.000
60-1i (b)	19.13	2,956	1,106	98.20	129.93
60-1i (c)	0.000	0.000	0.000	0.000	0.000
60-2c (a)	0.000	0.000	0.000	0.000	0.000
60-2c (b)	11.51	4,107	1,582	121.7	127.5
60-2c (c)	0.000	0.000	0.000	0.000	0.000
60-2i (a)	30.61	99.16	25.19	0.000	0.000
60-2i (b)	40.89	1,782	1,065	88.52	112.4
60-2i (c)	75.11	1,138	599.9	14.78	9.09
60-4i (a)	0.000	0.000	0.000	0.000	0.000
60-4i (b)	5.766	2,667	991.7	131.8	117.7
60-4i (c)	0.000	0.000	0.000	0.000	0.000
60-5c (a)	0.000	0.000	0.000	0.000	0.000
60-5c (b)	0.000	202.7	51.48	16.10	24.54
60-5c (c)	0.000	637.3	161.9	0.000	0.000
60-7c (a)	0.000	0.000	0.000	0.000	0.000
60-7c (b)	15.72	3,071	1,000	77.04	54.92
60-7c (c)	0.000	0.000	0.000	0.000	0.000
60-7i (a)	5.359	63.30	16.08	0.000	0.000
60-7i (b)	41.22	4,136	1,289	124.7	147.7
60-7i (c)	13.72	218.6	136.1	27.36	14.90
60-9c (a)	0.000	0.000	0.000	0.000	0.000
60-9c (b)	14.25	2,844	971.7	61.98	81.45
60-9c (c)	0.000	0.000	0.000	0.000	0.000

RESIDUAL STRENGTH EXPERIMENTS

Compressive residual strength experiments were conducted on all 27 subpanels, providing data to be related to each panels' quantified damage parameters.

Methods

The compressive residual strength experiments were conducted per ASTM D7137: Standard Test Method for Compressive Residual Strength Properties of Damaged Polymer Matrix Composite Plates [20] allowing for the calculation of ultimate compressive residual strength. Using a diamond blade wet saw, twenty-seven 101.6 mm x 152.4 mm (4 in x 6 in) subpanels were cut from the full-size panels after blast loading and imaging. Although all 304.8 mm x 304.8 mm (12 in x 12 in) panels had been painted for DIC prior to the blast experiments, the smaller subpanels required a denser speckle pattern. Additional black speckles were added to each subpanel to increase the speckle density, as shown in Figure 25.

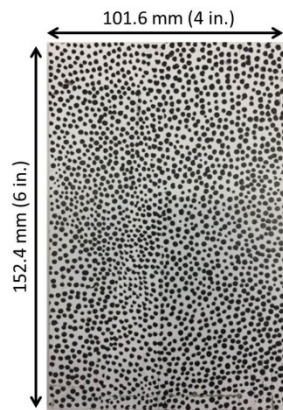


Figure 25. Subpanel cut and speckled for residual strength testing with DIC

For all residual strength experiments, two Prosilica GC2450 cameras were used to record images for 3D DIC throughout the test. Images were captured at 1 frame per

second, with a 50 mm lens, 512 x 512 resolution, and an aperture of 4.2. The specimen was mounted in a stabilizing fixture shown in Figure 26, which meets the guidelines of ASTM D7137.

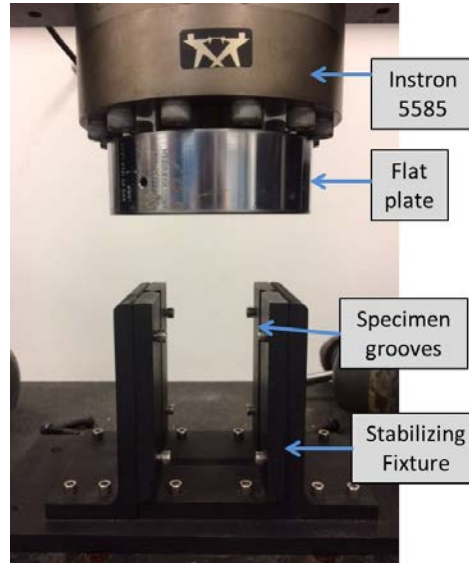


Figure 26. Compressive residual strength fixture mounted on INSTRON 5585

Compressive load and extension data were collected through the test machine, INSTRON 5585 and the accompanying Merlin software, while strain data was produced through 3D DIC. By combining these vectors in MATLAB, the ultimate compressive residual strength, σ_R , was calculated with Equation 9:

$$\sigma_R = \frac{P_{max}}{A_R} \quad (9)$$

where P_{max} is the maximum compressive load applied before failure (kN), and A_R is the cross-sectional area of the residual strength subpanel, 101.6 mm x 1.52 mm (4 in x 0.06 in). Each test was stopped once a failure occurred, identified by a load drop of at least 30% from P_{max} .

Per ASTM D7137, a test is considered valid if an acceptable failure mode is observed. Acceptable failure modes include delamination, cracking, brooming, or

explosive failure. End-crushing is not an acceptable failure mode, unless minor end-crushing occurs before final failure in the gage section [20]. Each subpanel was evaluated after the test to determine if a valid test had occurred. Only valid test specimens may be included in the development of the damage-strength relationship.

Results

The ultimate compressive residual strength was calculated in MATLAB using data from the INSTRON 5585 and 3D DIC. The test setup is shown in Figure 27.

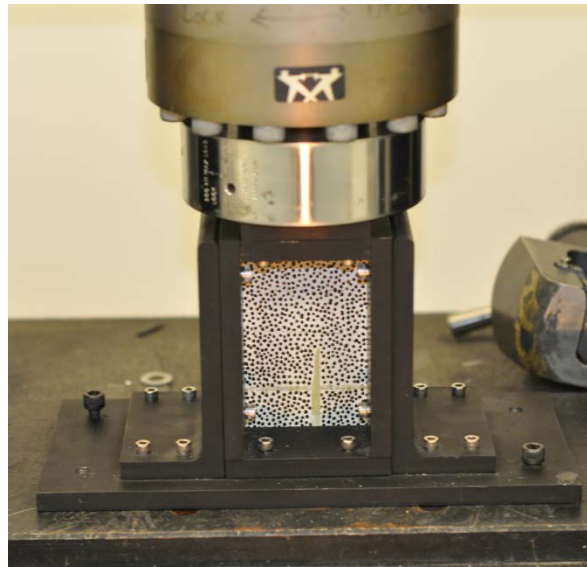


Figure 27. Residual strength test setup with speckled subpanel mounted

Of the 27 subpanels tested, 10 did not have any reported damage, as previously shown in Table 3. Since ASTM D 7137 is designed to test the residual strength of damaged composites, it was expected that these 10 panels would not have acceptable failure modes. These 10 panels, as well as 3 other subpanels that only had minor amounts of damage, failed due to end-crushing at the top boundary, as shown in Figure 28.

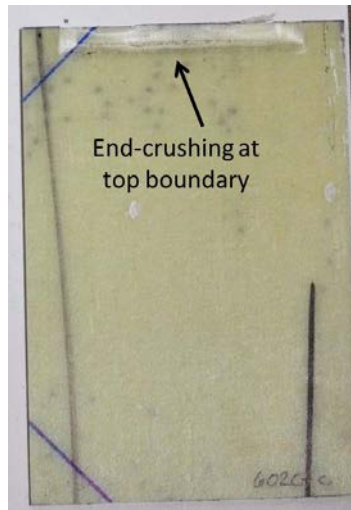


Figure 28. End-crushing from residual strength test on low-damage subpanel 60-2c (c)

End-crushing is not an acceptable failure mode, creating 13 invalid residual strength tests. The remaining 14 subpanels had acceptable failure modes, as shown for 60-2i (c) in Figure 29.

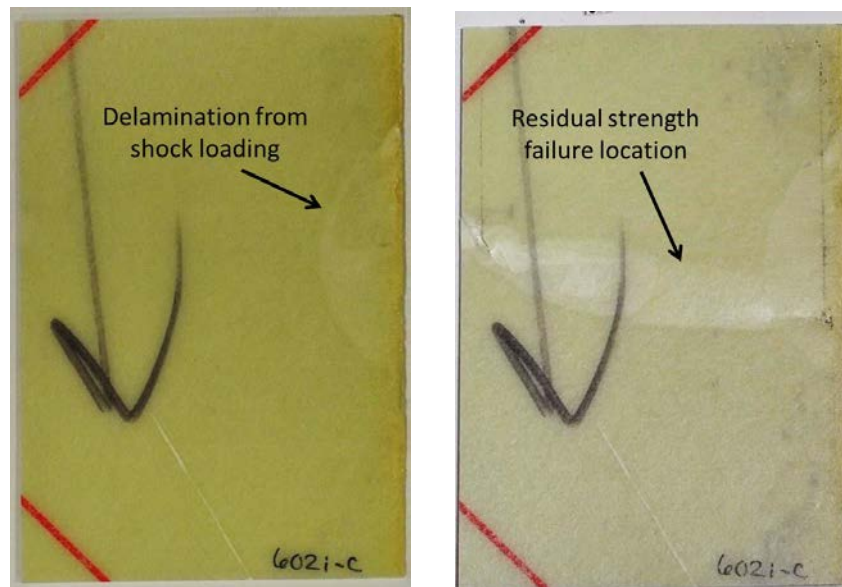


Figure 29. Subpanel 60-2i (c) before (left) and after (right) residual strength test, showing an acceptable failure mode initiating at damage location

The results show that the residual strength varies for panels with different amounts of shock damage. It was observed that panels with little or no damage failed

via end-crushing around 88.25 ± 6.2 MPa (12.8 ± 0.9 ksi), as was shown in Figure 28. Furthermore, subpanels with significant amounts of reported damage had residual strengths as low as 21.82 MPa (3.164 ksi), seen in subpanel 60-1c (a). All 27 panels, regardless of an acceptable or unacceptable failure mode, demonstrated similar behaviors in the load-displacement curves. Most panels had some minor intermediate drops in load, either from fiber buckling or adjustments in the fixture. However, since the stop criteria for the test was defined as a load drop of least 30% from P_{max} , the test continued past these minor load drops. Figure 30 shows the load-displacement curves for 60-2c (c) and 60-2i (c), which had minor and significant amounts of damage, respectively. The load-displacement curve for 60-2c (c) plateaus around 13 kN before dropping, indicative of boundary crushing; however, 60-2i (c) drops suddenly. These curves demonstrate typical behaviors observed throughout the test series. Subpanels with more damage consistently failed at lower loads.

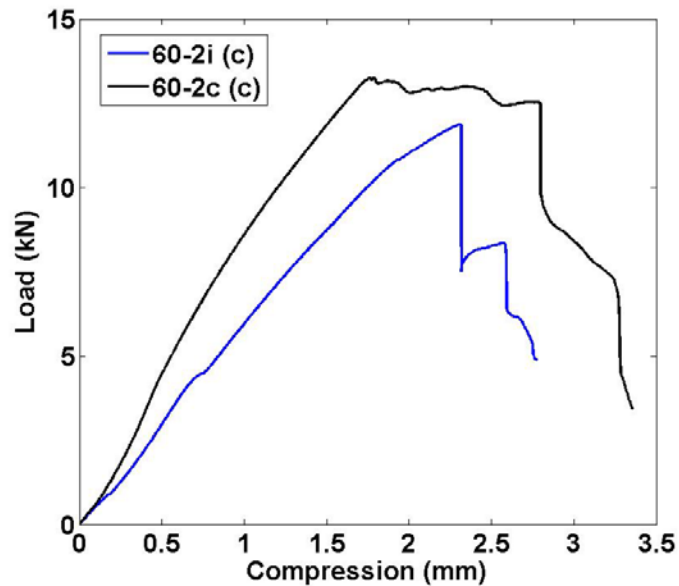


Figure 30. Load-displacement curves for residual strength tests of subpanels 60-2i (c) and 60-2c (c) showing acceptable and unacceptable failure modes

Table 4 shows the results of the residual strength tests, and identifies which 14 subpanels had acceptable failure modes.

Table 4. Compressive residual strengths, σ_R , for all subpanels

Subpanel	Compressive Residual Strength, σ_R (MPa)	Compressive Residual Strength, σ_R (ksi)	Acceptable Failure Mode (Yes/No)
60-1c (a)	46.82	6.789	Yes
60-1c (b)	21.82	3.164	Yes
60-1c (c)	69.55	10.09	Yes
60-2c (a)	87.99	12.76	No
60-2c (b)	42.20	6.119	Yes
60-2c (c)	85.61	12.41	No
60-5c (a)	95.83	13.90	No
60-5c (b)	62.53	9.067	Yes
60-5c (c)	74.14	10.75	Yes
60-7c (a)	84.77	12.29	No
60-7c (b)	88.26	12.80	No
60-7c (c)	86.17	12.49	No
60-9c (a)	90.39	13.11	No
60-9c (b)	92.23	13.37	No
60-9c (c)	94.04	13.64	No
60-1i (a)	67.10	9.730	Yes
60-1i (b)	49.71	7.207	Yes
60-1i (c)	73.87	10.71	No
60-2i (a)	97.51	14.14	No
60-2i (b)	39.60	5.742	Yes
60-2i (c)	76.60	11.11	Yes
60-4i (a)	82.76	12.00	No
60-4i (b)	76.64	11.11	Yes
60-4i (c)	89.96	13.04	No
60-7i (a)	82.90	12.02	Yes
60-7i (b)	53.89	7.815	Yes
60-7i (c)	76.70	11.12	Yes

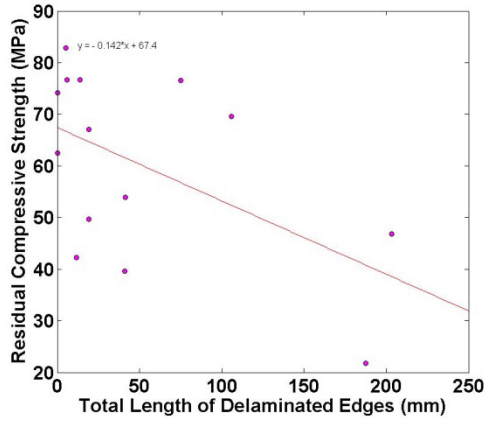
The residual strength experiments yielded 14 valid data points for the development of a damage-strength relationship.

RELATIONSHIP BETWEEN DAMAGE AND RESIDUAL STRENGTH

The damage quantities, $[d_i]$, reported in Table 3, and the residual strengths, $[\sigma_R]$, reported in Table 4, were imported into MATLAB to develop a prediction equation for residual strength in shock-damaged Cyply 1002 laminate panels.

Correlation of Individual Damage Parameters

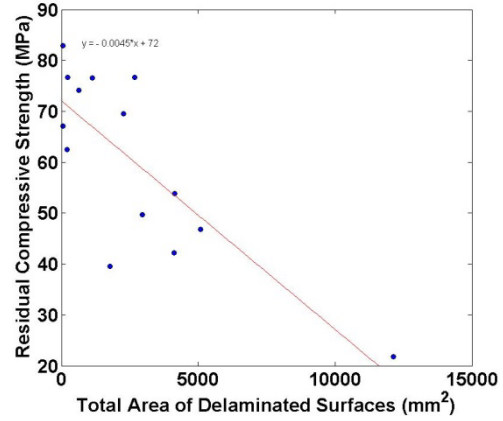
As shown in Figure 31, scatter plots were created in MATLAB to show the correlation between the residual strength data, and each of the five damage vectors— $[d_1]$, total length of delaminated edges (mm), $[d_2]$, total area of delaminated surfaces (mm^2), $[d_3]$, total volume of delaminated regions (mm^3), $[d_4]$, total length of cracks (mm), and $[d_5]$, total surface area of cracks (mm^2). For each damage quantity, Figure 31 also provides the correlation, c , and the slope, m , and intercept, b , of the linear best-fit line.



$$c_1 = -0.5353$$

$$m_1 = -0.1420$$

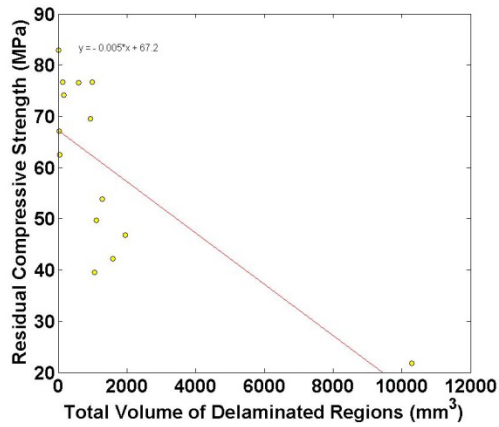
$$b_1 = 67.40$$



$$c_2 = -0.7967$$

$$m_2 = -0.0045$$

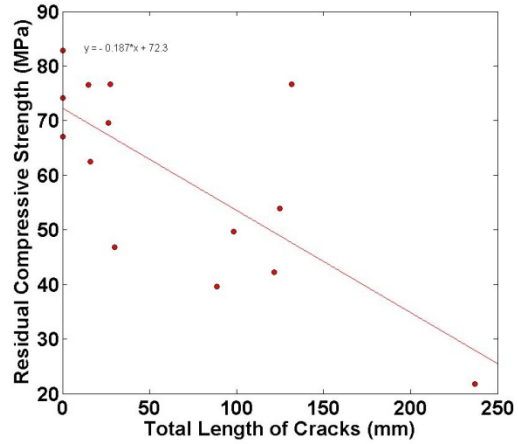
$$b_2 = 72.01$$



$$c_3 = -0.7293$$

$$m_3 = -0.0050$$

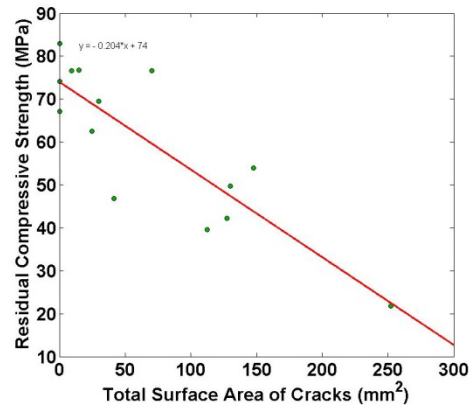
$$b_3 = 67.23$$



$$c_4 = -0.7305$$

$$m_4 = -0.1871$$

$$b_4 = 72.26$$



$$c_5 = -0.8549$$

$$m_5 = -0.2042$$

$$b_5 = 74.01$$

Figure 31. Individual damage quantities plotted against residual strength with calculated correlations and linear best-fit lines

A single damage parameter cannot fully predict residual strength, as shown by the correlations, c_i . Therefore, a combined damage parameter can be created that has a stronger correlation with the residual strength data.

Combined Damage Parameter

This section describes a method (Method 1) for defining a combined damage parameter, d_c ; alternative methods for defining d_c (Methods 2a and 2b) are provided in Appendix C.

Before creating a combined damage parameter using Method 1, the five initial damage quantities were evaluated for redundancy. By calculating the correlations between each individual damage quantity, it was confirmed that $[d_2]$, the total area of delaminated surfaces and $[d_3]$, the total volume of delaminated regions were highly dependent on one another, with a correlation of 0.9486. Additionally, $[d_4]$, the total length of cracks, and $[d_5]$, the total surface area of cracks were also found to be highly dependent on each other, with a correlation of 0.9558. Therefore, $[d_3]$ and $[d_4]$ were discarded from the creation of the combined damage parameter, leaving three damage parameters, $[d_j]$: $[d_1]$, $[d_2]$, and $[d_5]$.

In order to appropriately weight each damage parameter within the equation for the combined damage parameter, $[d_c]$, their correlations were normalized. The normalized correlations, \bar{c}_j , which serve as weight values for the combined damage parameter, are defined by Equation 10:

$$\bar{c}_j = \frac{c_j}{\sum c_j} \quad (10)$$

$$\bar{c}_1 = \frac{c_1}{c_1 + c_2 + c_5} = 0.2448$$

$$\bar{c}_2 = \frac{c_2}{c_1 + c_2 + c_5} = 0.3643$$

$$\bar{c}_5 = \frac{c_5}{c_1 + c_2 + c_5} = 0.3909$$

Using the normalized correlations as parameter weights, and the slopes shown in Figure 31, a combined damage parameter, $[d_c]$, can be defined using Equation 11:

$$[d_c] = \frac{m_1 \bar{c}_1 [d_1] + m_2 \bar{c}_2 [d_2] + m_5 \bar{c}_5 [d_5]}{m_1 + m_2 + m_5}$$

$$[d_c] = \frac{-0.0348 [d_1] - 0.00164 [d_2] - 0.0798 [d_5]}{-0.3507} \quad (11)$$

Figure 32 shows $[d_c]$ versus the residual strength data, $[\sigma_R]$, for Method 1. The data points for each fiber orientation—crossply and isotropic—are shown in the plot; however, the data did not demonstrate a significant difference in behavior or residual strength for the different fiber orientations. However, future work with additional experiments may highlight a trend for the two fiber orientations.

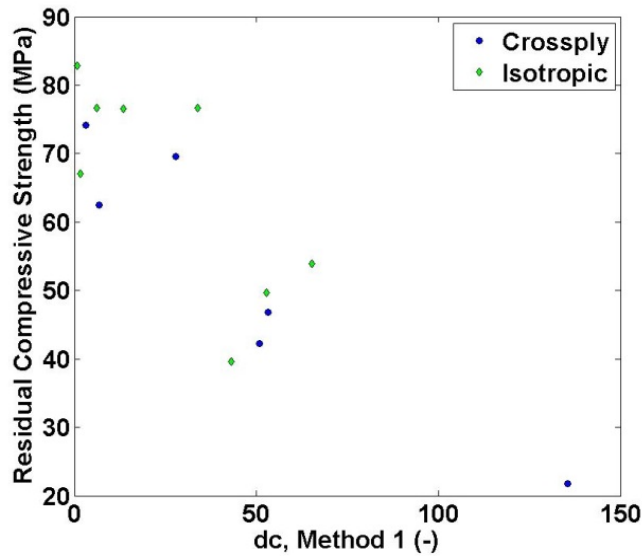


Figure 32. Scatter plot of combined damage parameter, $[d_c]$, versus residual strength, σ_R

The correlation between $[d_c]$ and $[\sigma_R]$ is defined as c_{dc} , and is stronger than those of the initial damage parameters shown in Figure 31:

$$c_{dc} = -0.8580$$

Prediction Equation

A linear prediction equation is produced using: the combined damage parameter, d_c , which is a function of total length of edge delamination, d_1 , total surface area of delamination d_2 , and the total surface area of cracks, d_5 ; the sum, m_c , of the slopes of the best fit lines for d_1 , d_2 , and d_5 versus σ_R ; and the average, B_c , of the y-intercepts of the best fit lines for d_1 , d_2 , and d_5 versus σ_R :

$$[d_c] = \frac{-0.0348[d_1] - 0.00164[d_2] - 0.0798[d_5]}{-0.3507} \quad (12)$$

$$m_c = m_1 + m_2 + m_5 = -0.3507 \quad (13)$$

$$B_c = \frac{b_1 + b_2 + b_5}{3} = 71.1 \text{ MPa} \quad (14)$$

Therefore, for a Cyply 1002 composite laminate with damage quantities determined through visual inspection, FIRT, or THz imaging, the compressive residual strength, σ_R , can be predicted by Equation 15:

$$[\sigma_R] = m_c[d_c] + B_c$$

$$[\sigma_R] = -0.3507 * [d_c] + 71.1 \text{ MPa} \quad (15)$$

The correlation between this prediction equation and the actual residual strength data is -0.8580.

Additionally, in the case that eliminating redundant parameters is complex or non-obvious, an alternative method has been developed using a principal component

analysis to create the combined damage parameter, $[d_c]$. This method is described in Appendix C. The MATLAB code for developing this prediction equation, with both methods, is provided in Appendix D.

CONCLUSIONS

Experiments and non-destructive imaging were conducted to investigate the effects of shock loading on a composite structure's compressive residual strength. Shock tube experiments, residual strength tests, and material characterization tests were conducted at URI's Dynamic Photomechanics Laboratory; non-destructive imaging of Cyply 1002 glass-fiber/epoxy laminates was conducted at the Naval Undersea Warfare Center Division, Newport. The research yields the following conclusions:

- Non-destructive imaging technologies—Flash Infrared Thermography (FIRT) and Terahertz (THz) — were used to obtain through-thickness images of composite laminate panels, before and after shock-induced damage.
- FIRT and THz data was used to quantify damage in glass fiber/epoxy composite panels (Cyply 1002) in terms of the following quantities:
 - Total length of delaminated edges
 - Total area of delaminated surfaces—internal and external
 - Total volume of delaminated regions
 - Total length of cracks
 - Total surface area of cracks
- Residual strength experiments, conducted on shock-loaded composite panels, show that increased shock damage causes a reduction in compressive residual strength.

- The five damage parameters quantified through FIRT and THz imaging were combined and weighted in MATLAB to create one comprehensive damage parameter, d_c .
- A relationship was developed to predict the compressive residual strength, σ_R , of a Cyply 1002 laminate panel, using the combined damage parameter, d_c . The prediction equation has a strong negative correlation (-0.8580) to the data collected during the residual strength experiments.

Future work will include additional blast experiments, imaging, data quantification, and residual strength testing—in order to validate and refine the prediction equation determined in this thesis. Additional blast experiments will be conducted with different incident pressures, to induce a wider range of damage and fill in gaps on the plots for residual strength versus damage. With additional data, differences between crossply and isotropic fiber orientations may become clear; in this case, separate prediction equations may be necessary. Now that this thesis has developed a methodology for evaluating damage and residual strength of composite materials, future work may follow this methodology for a variety of composite materials and thicknesses. Additionally, since this research studied the residual compressive strength after blast, future work may evaluate the residual tensile or flexural strength after blast loading.

LIST OF REFERENCES

- [1] D. F. Adams, L. A. Carlsson, and R. B. Pipes, *Experimental Characterization of Advanced Composite Material*, Third. CRC Press, 2003.
- [2] J. LeBlanc, C. Shillings, E. Gauch, F. Livolsi, and A. Shukla, “Near Field Underwater Explosion Response of Polyurea Coated Composite Plates,” *Exp. Mech.*, vol. 56, no. 4, pp. 569–581, Apr. 2016.
- [3] J. LeBlanc, A. Shukla, C. Rousseau, and A. Bogdanovich, “Shock loading of three-dimensional woven composite materials,” *Compos. Struct.*, vol. 79, no. 3, pp. 344–355, Jul. 2007.
- [4] J. LeBlanc, “Experimental Evaluation of Novel Composites for Use in Transport of Explosive Materials,” University of Rhode Island, 2005.
- [5] V. K. Kannan, A. Rajadurai, and B. N. Rao, “Residual strength of laminated composites after impact,” *J. Compos. Mater.*, vol. 45, no. 9, pp. 1031–1043, 2011.
- [6] D. E. Pettit, K. N. Lauraitis, J. M. Cox, and L.-C. C. O. BURBANK., *Advanced Residual Strength Degradation Rate Modeling for Advanced Composite Structures. Volume 1. Task I: Preliminary Screening*. Defense Technical Information Center, 1979.
- [7] G. L. Farley, “Effect of low-velocity or ballistic impact damage on the strength of thin composite and aluminum shear panels,” National Aeronautics and Space Administration, Scientific and Technical Information Branch, 1985.
- [8] E. Saether, “RESTRAN: Residual Strength Analysis of Impact Damaged Composite Laminates Volume I: Theoretical Manual,” 2001.

- [9] J.-M. Koo, J.-H. Choi, and C.-S. Seok, "Evaluation for residual strength and fatigue characteristics after impact in CFRP composites," *Compos. Struct.*, vol. 105, pp. 58–65, Nov. 2013.
- [10] A. Ruiz, "Residual Strength After Fatigue of a Cross-Ply Metal Matrix Composite at Elevated Temperature," AIR FORCE INST OF TECH WRIGHT-PATTERSON AFB OH, 1997.
- [11] H. Arora *et al.*, "Compressive strength after blast of sandwich composite materials," *Philosophical transactions. Series A, Mathematical, physical, and engineering sciences*, vol. 372, no. 2015. May-2014.
- [12] "ASTM D3039/D3039M-17 Standard Test Method for Tensile Properties of Polymer Matrix Composite Materials." ASTM International, West Conshohocken, PA, 2017.
- [13] "ASTM D7264/D7264M-15 Standard Test Method for Flexural Properties of Polymer Matrix Composite Materials." ASTM International, West Conshohocken, PA, 2015.
- [14] "ASTM D3410/D3410M-16 Standard Test Method for Compressive Properties of Polymer Matrix Composite Materials with Unsupported Gage Section by Shear Loading." ASTM International, West Conshohocken, PA, 2016.
- [15] S. M. Badiger, "Design and Fabrication of an Experimental Facility for Controlled, Transient Shock Wave Loading," University of Rhode Island, 2004.
- [16] P. Kumar, J. LeBlanc, D. S. Stargel, and A. Shukla, "Effect of plate curvature on blast response of aluminum panels," *Int. J. Impact Eng.*, vol. 46, pp. 74–85, Aug. 2012.

- [17] H. Schreier, J. J. Orteu, and M. A. Sutton, *Image correlation for shape, motion and deformation measurements: Basic concepts, theory and applications*. 2009.
- [18] A. Shukla and J. W. Dally, *Experimental Solid Mechanics*, Second. Knoxville, TN: College House Enterprises, LLC, 2014.
- [19] P. Lockhart, “Terahertz Imaging Nondestructive Maintenance Inspections (Distribution Statement A).” Naval Undersea Warfare Center Division, Newport, 2015.
- [20] “ASTM D7137/D7137M-17 Standard Test Method for Compressive Residual Strength Properties of Damaged Polymer Matrix Composite Plates.” ASTM International, West Conshohocken, PA, 2017.

**APPENDIX A: PANEL IMAGES BEFORE, DURING, AND AFTER SHOCK
TUBE EXPERIMENTS**

High-speed photographs, DIC displacement contours, and damaged photographs are shown for all panels exposed to shock tube experiments.

60-1c

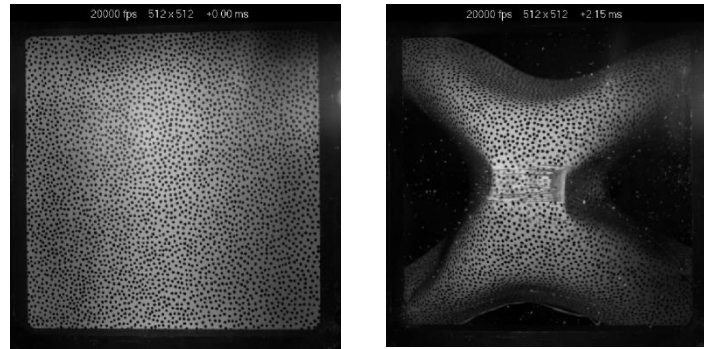


Figure 33. 60-1c Panel images before and during blast using high speed cameras

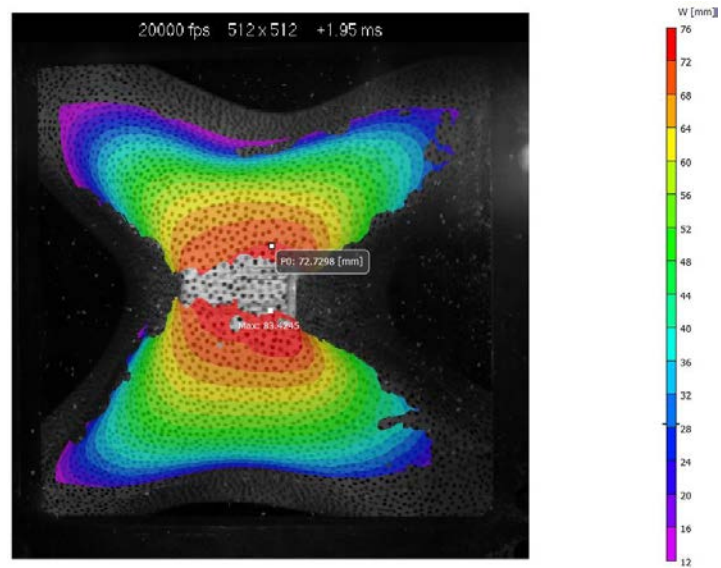


Figure 34. Maximum out-of-plane displacement for 60-1c

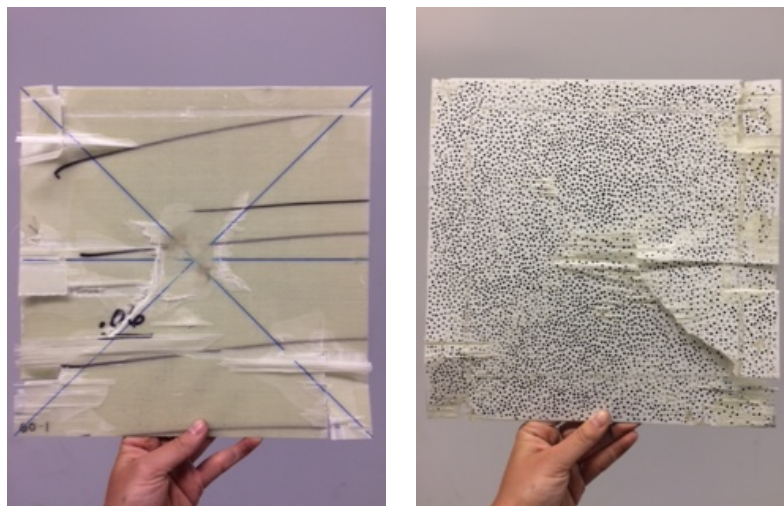


Figure 35. 60-1c damaged after blast loading (front, back)

60-2c

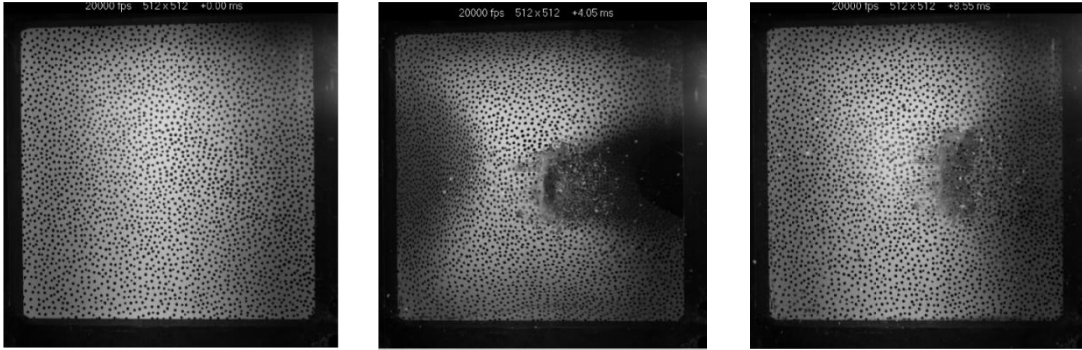


Figure 36. 60-2c Panel images before, during, and after blast using high speed cameras

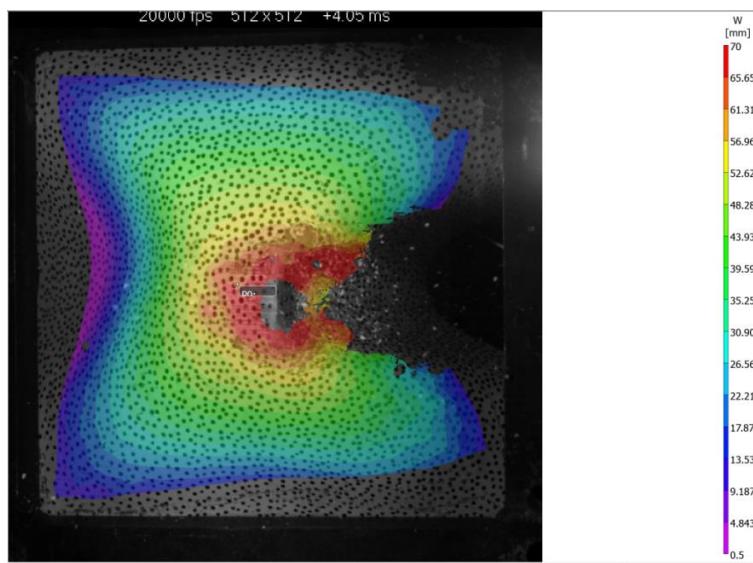


Figure 37. Maximum out-of-plane displacement for 60-2c

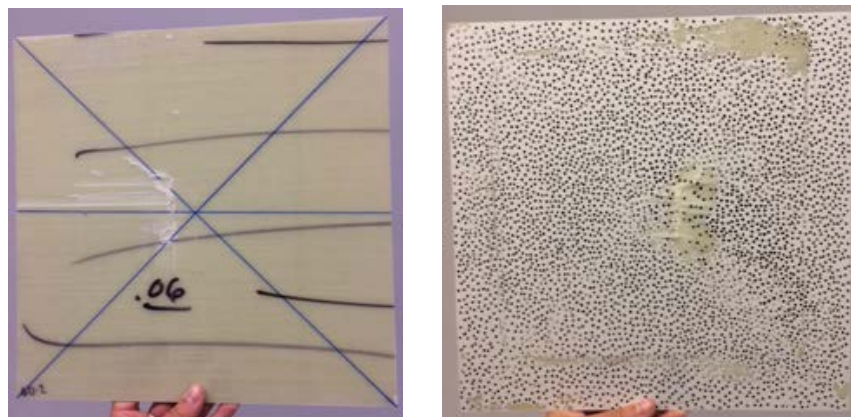


Figure 38. 60-2c damaged after blast loading (front, back)

60-5c

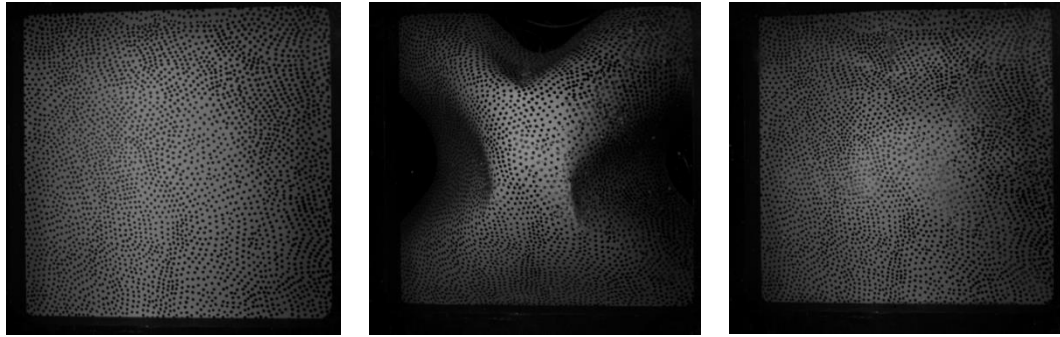


Figure 39. 60-5c panel images before, during, and after blast using high speed cameras

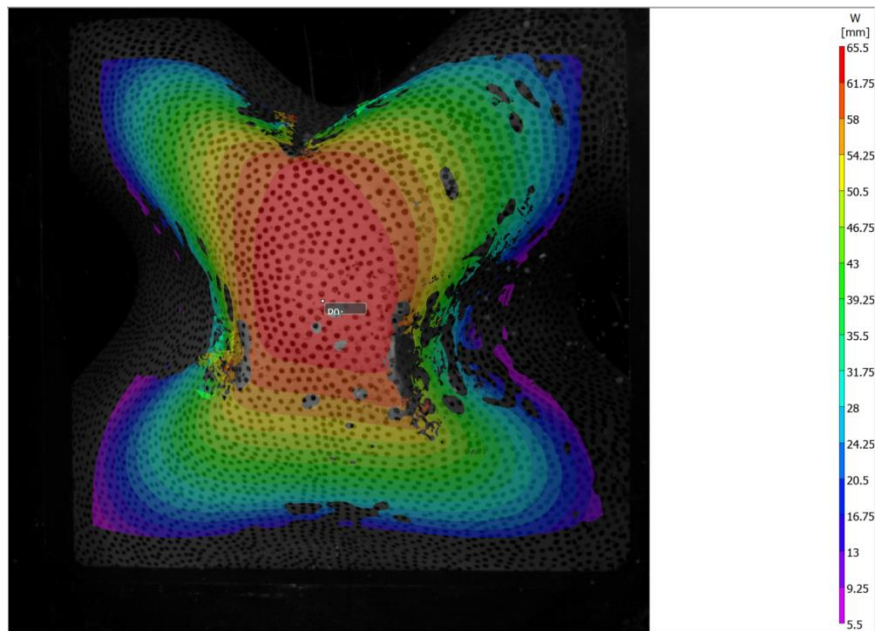


Figure 40. Maximum out-of-plane displacement for 60-5c

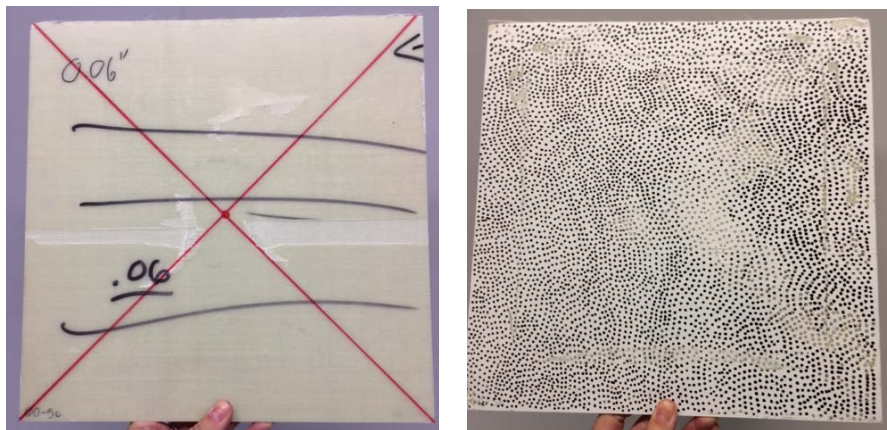


Figure 41. 60-5c damage after blast loading (front, back)

60-7c

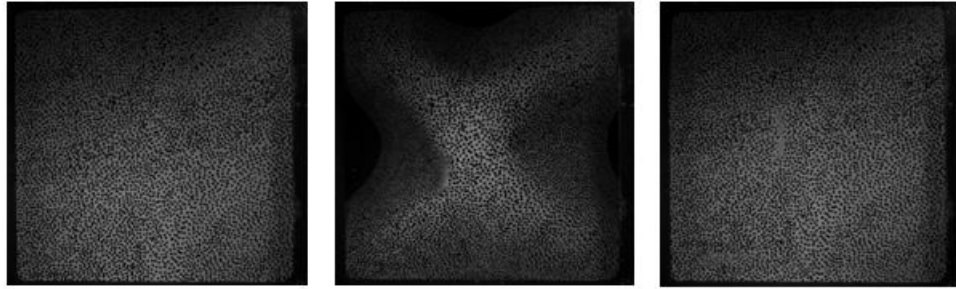


Figure 42. 60-7c panel images before, during, and after blast using high speed cameras

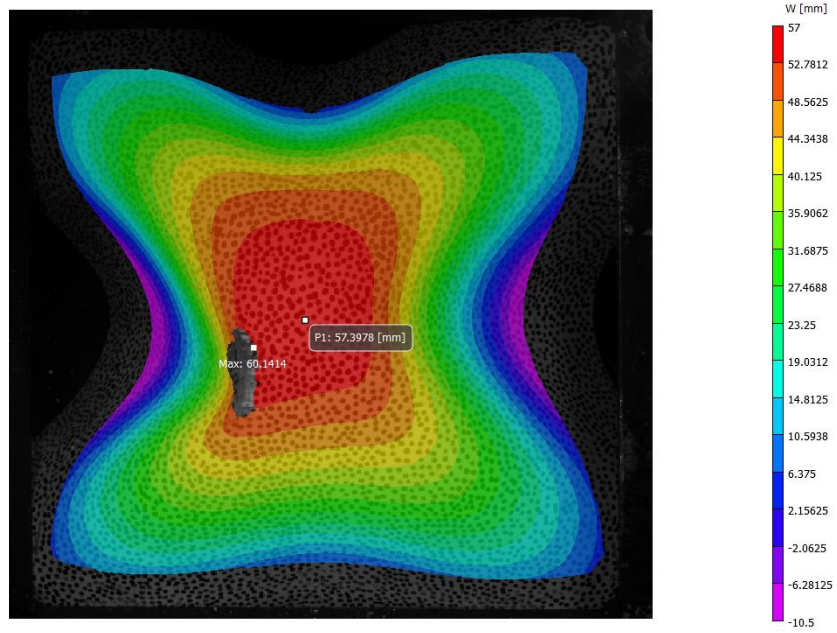


Figure 43. maximum out-of-plane displacement for 60-7c

60-9c



Figure 44. 60-9c panel images before, during, and after blast using high speed cameras

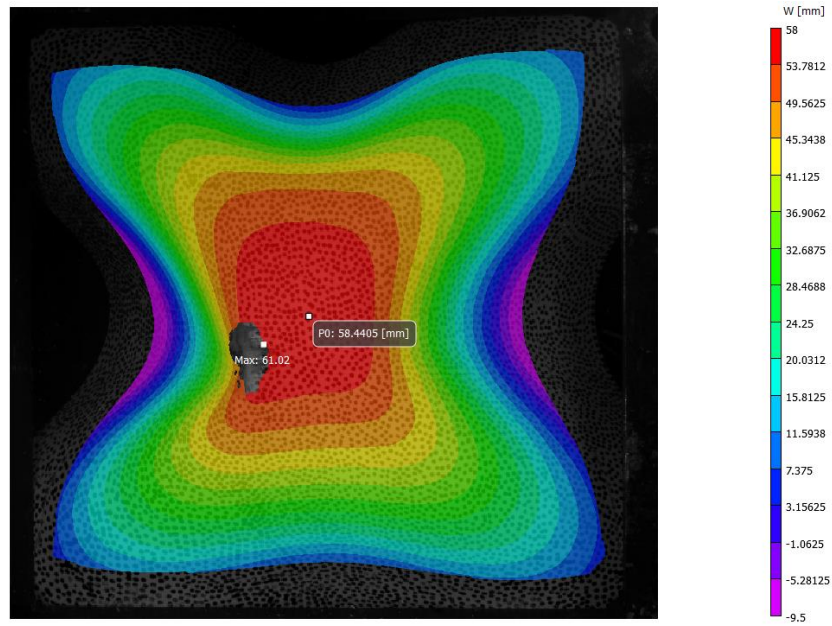


Figure 45. Maximum out-of-plane displacement for 60-9c

60-1i

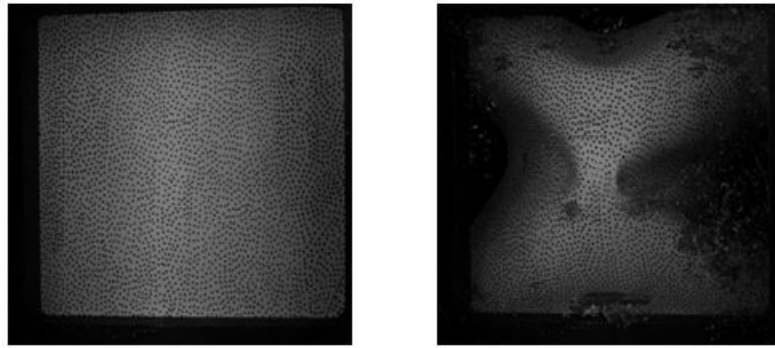


Figure 46. 60-1i panel images before and during blast using high speed cameras

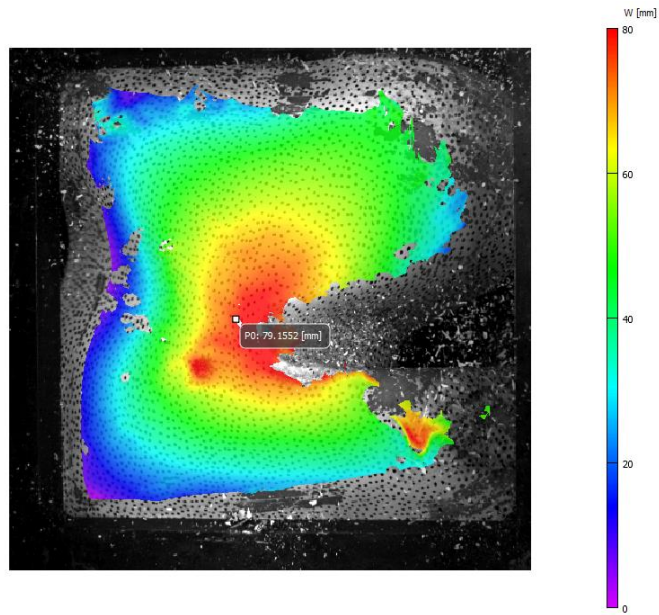


Figure 47. Maximum out-of-plane displacement for 60-1i

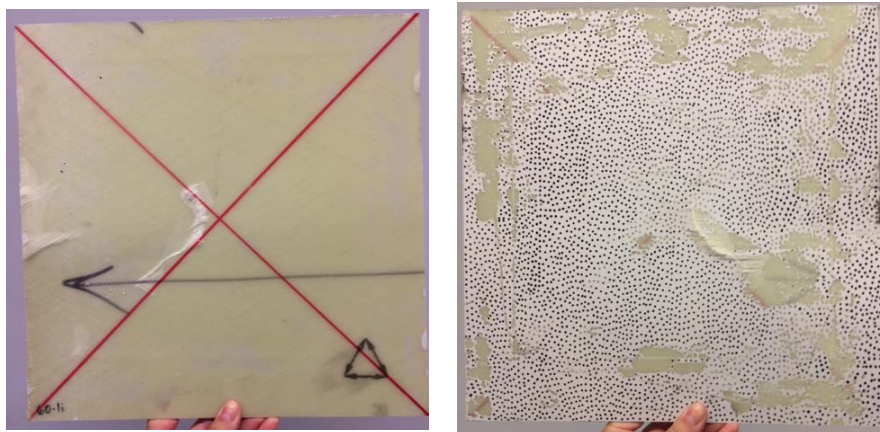


Figure 48. 60-1i damage after blast loading (front, back)

60-2i

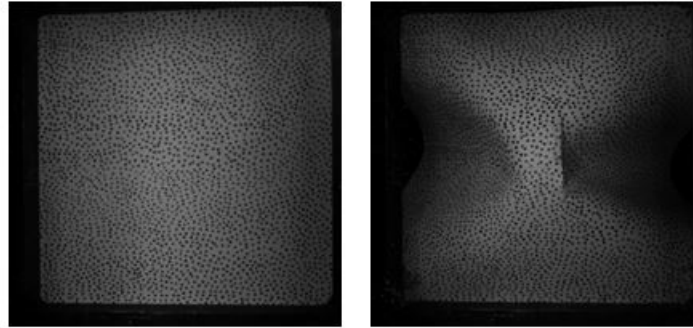


Figure 49. 60-2i panel images before and during blast using high speed cameras

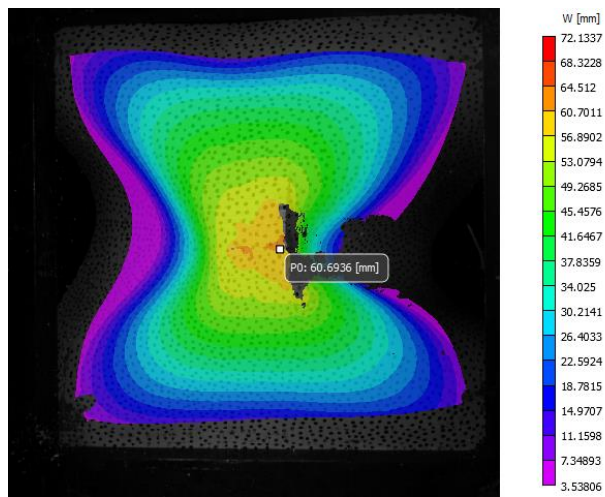


Figure 50. Maximum out-of-plane displacement for 60-2i

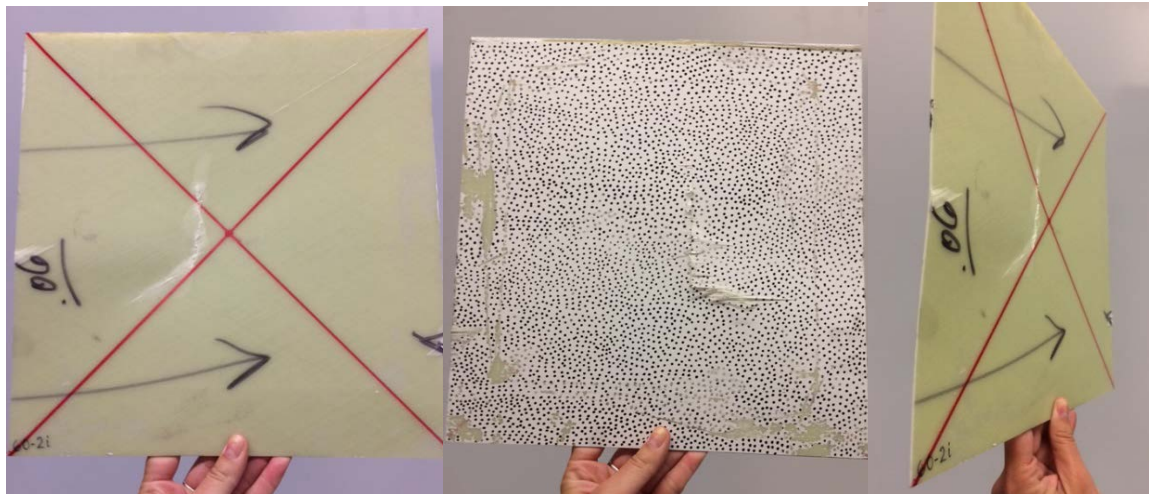


Figure 51. 60-2i damage after blast loading (front, back, side)

60-4i

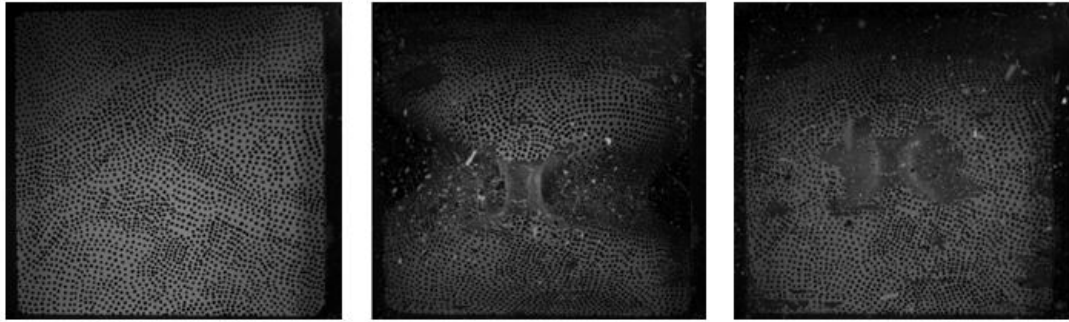


Figure 52. 60-4i panel images before, during, and after blast using high speed cameras

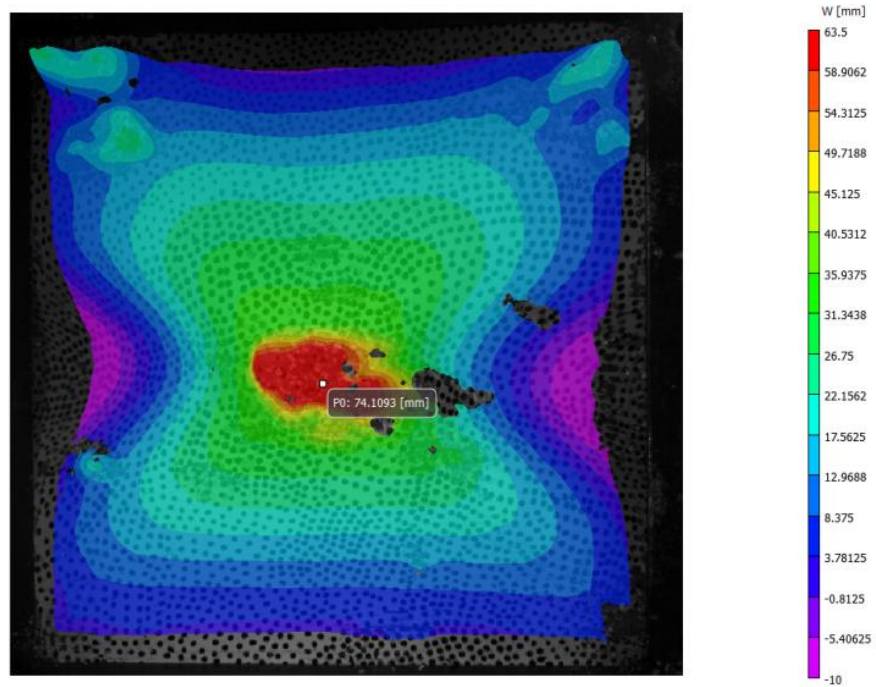


Figure 53. Maximum out-of-plane displacement for 60-4i

60-7i

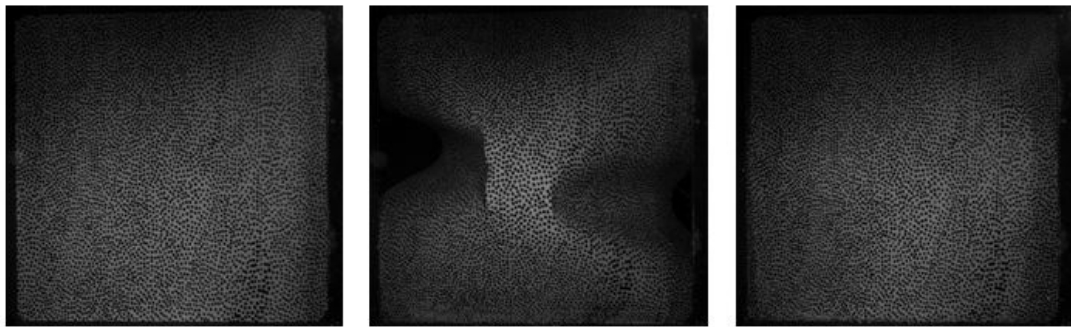


Figure 54. 60-7i panel images before, during, and after blast using high speed cameras

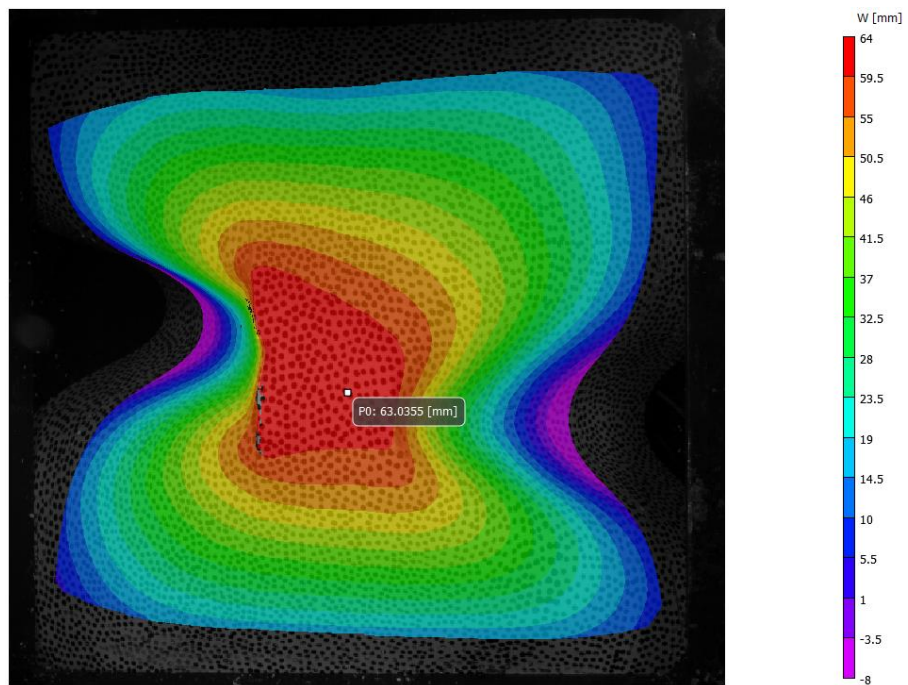
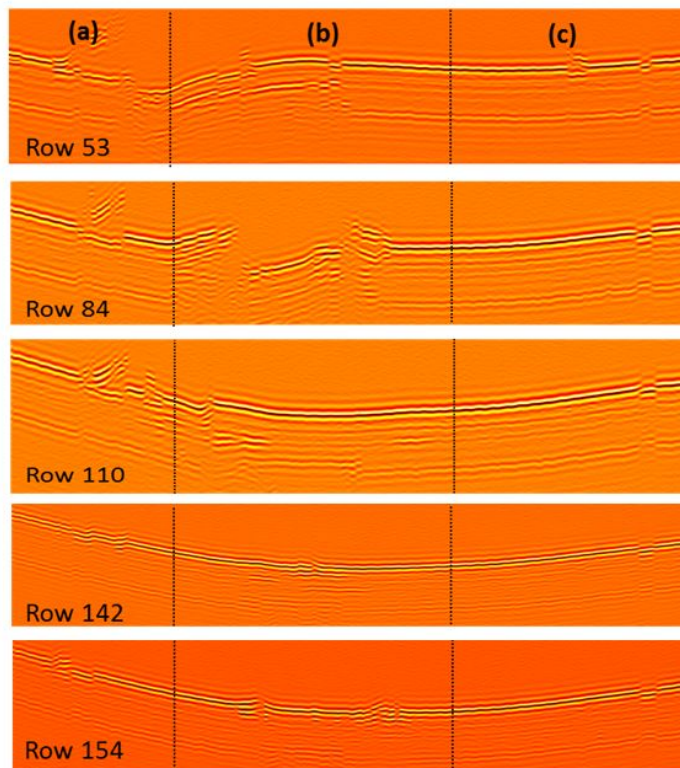
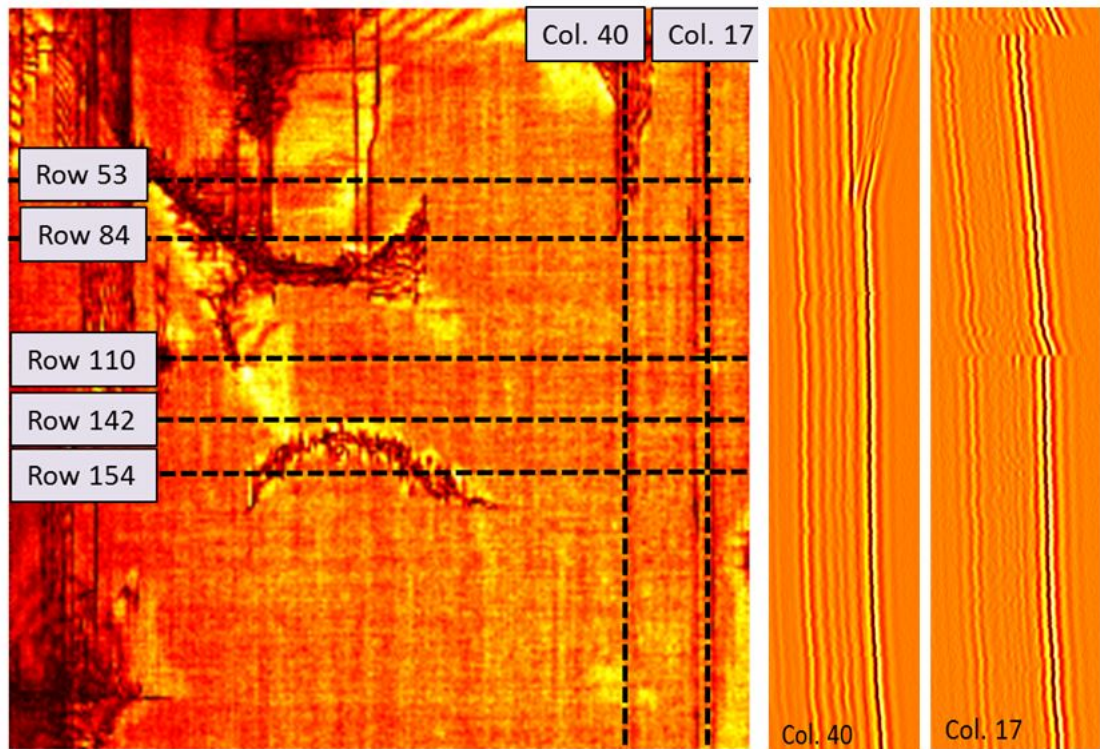


Figure 55. Maximum out-of-plane displacement for 60-7i

**APPENDIX B: TERAHERTZ (THZ) AND FLASH INFRARED
THERMOGRAPHY (FIRT) IMAGES FOR ALL PANELS**

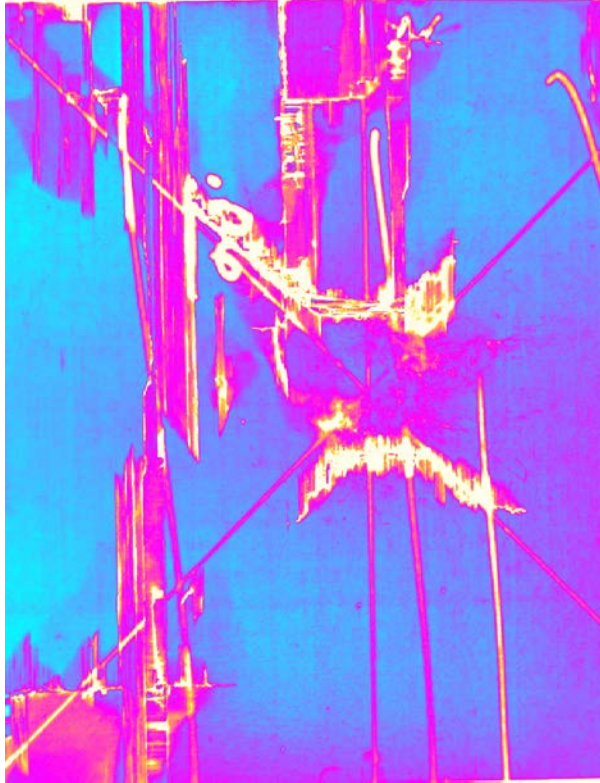
FIRT and THz images are shown for all damaged panels after exposure to shock loading.

60-1c

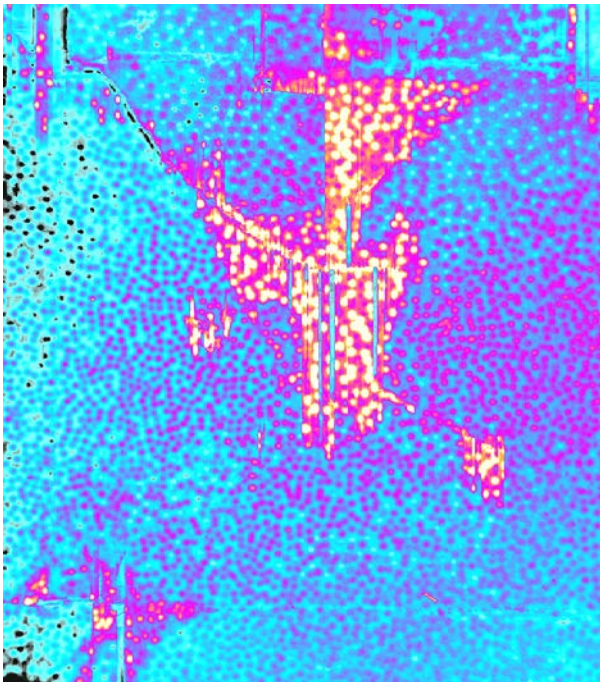


60-1c, continued

Front Face (TSR):

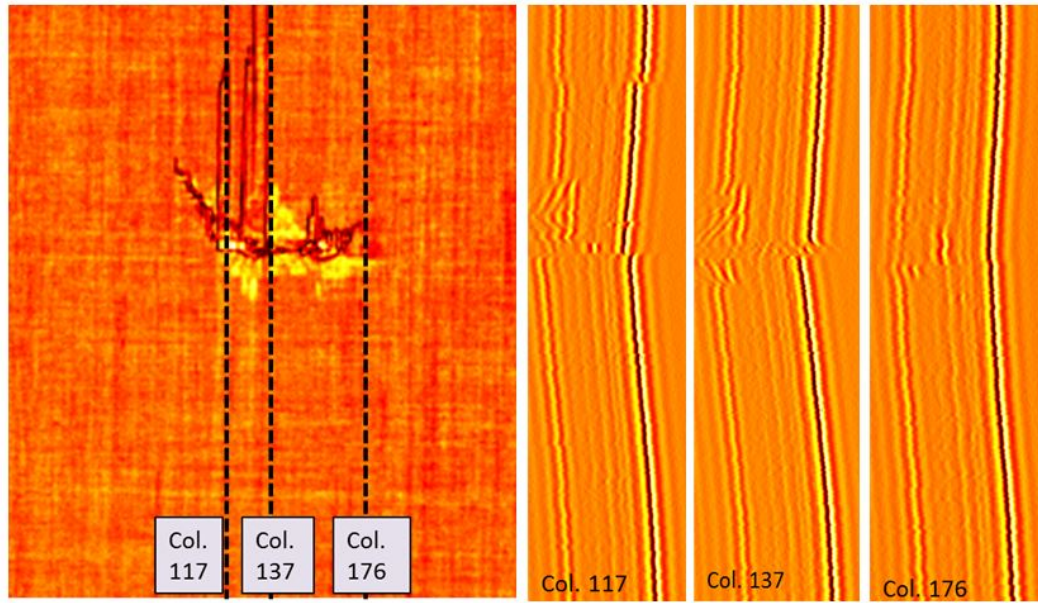


Back Face (TSR):

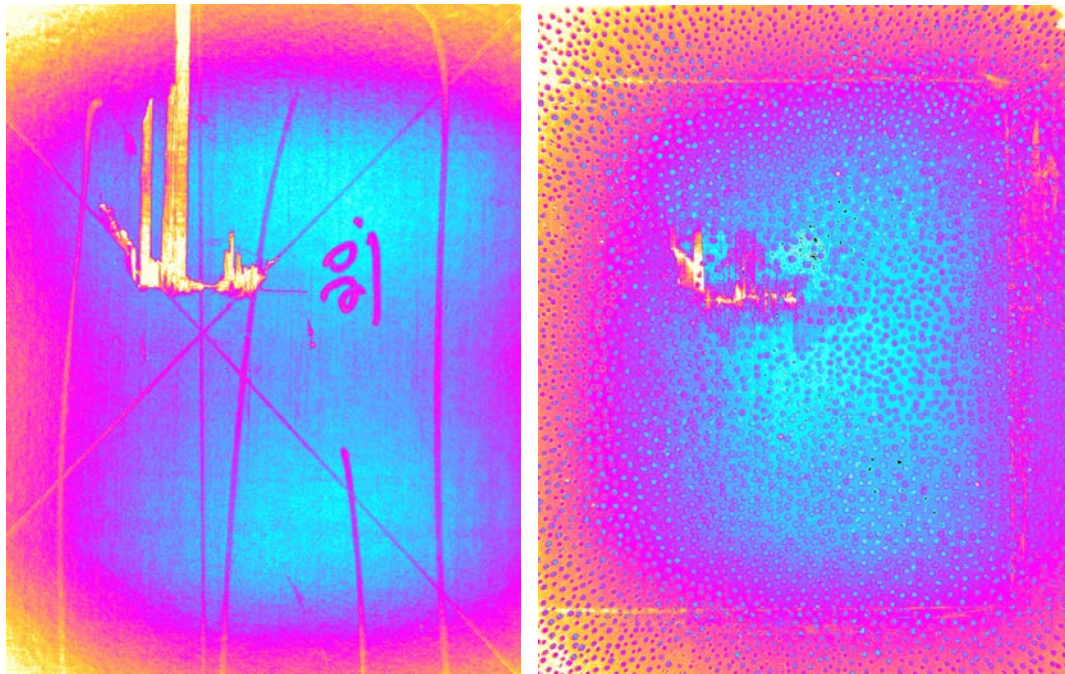


60-2c

THz (signal intensity map, column depth scans):

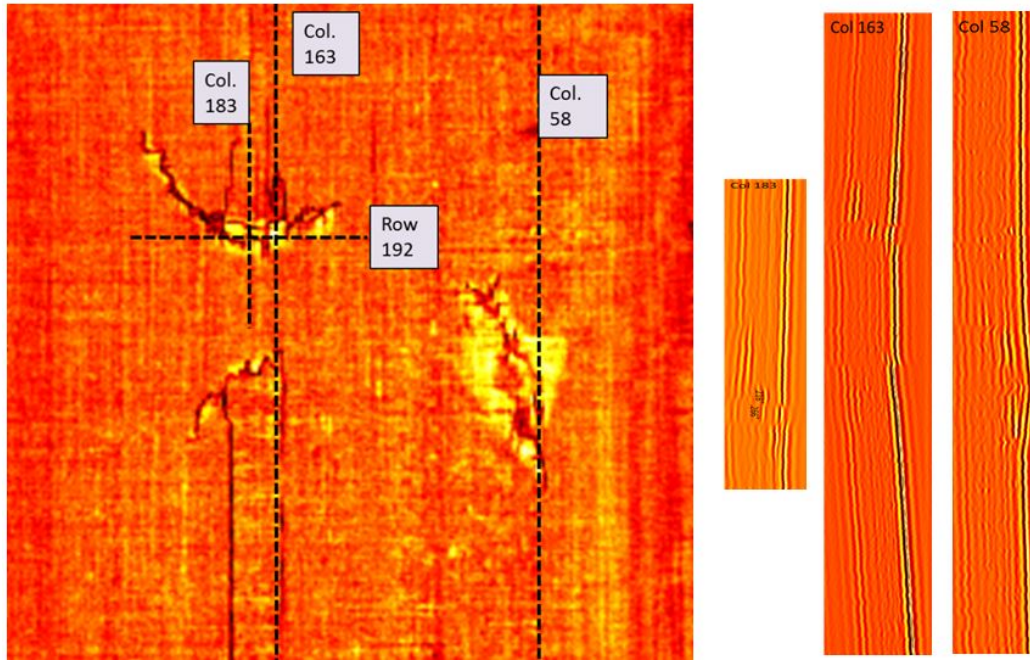


FIRT (front face 1d, back face 1d):



60-5c

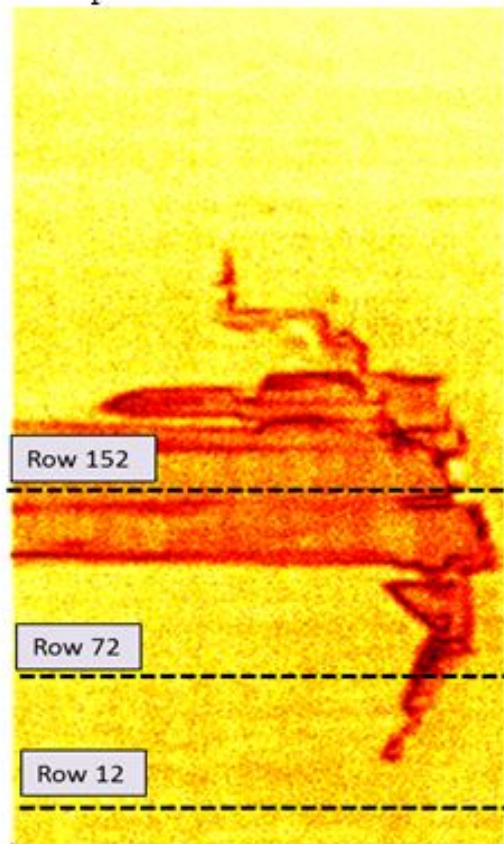
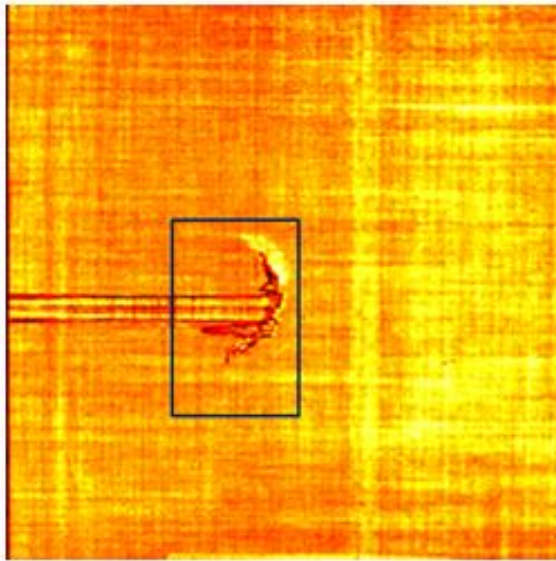
THz (signal intensity map, column depth scans):



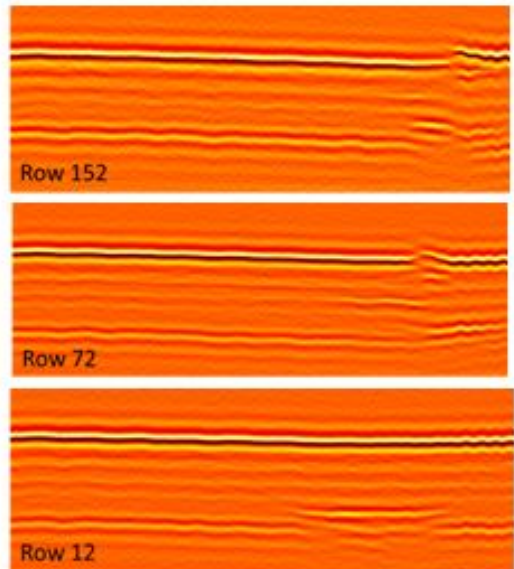
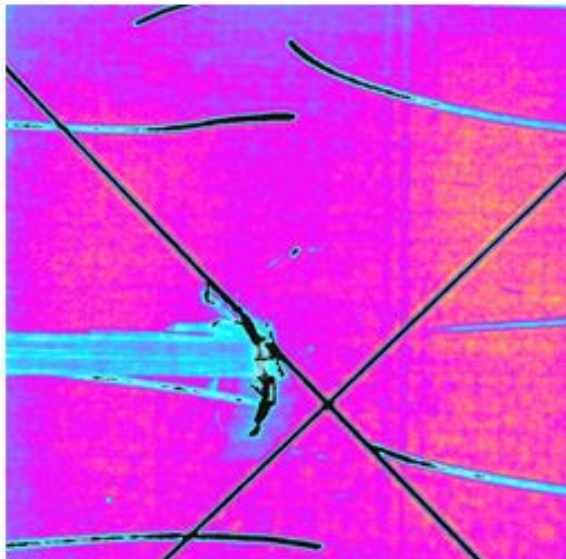
FIRT (front face TSR):



60-7c

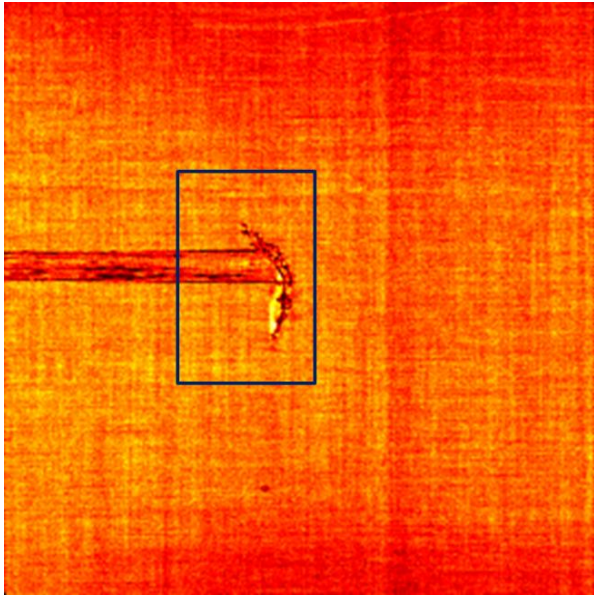


FIRT (1d):

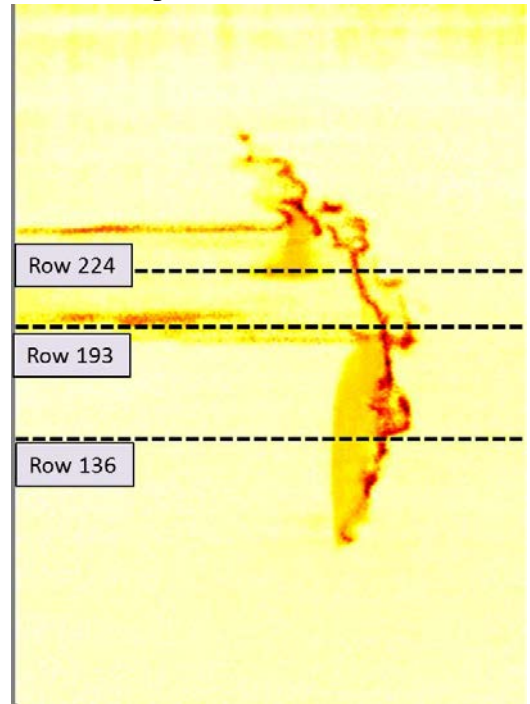


60-9c

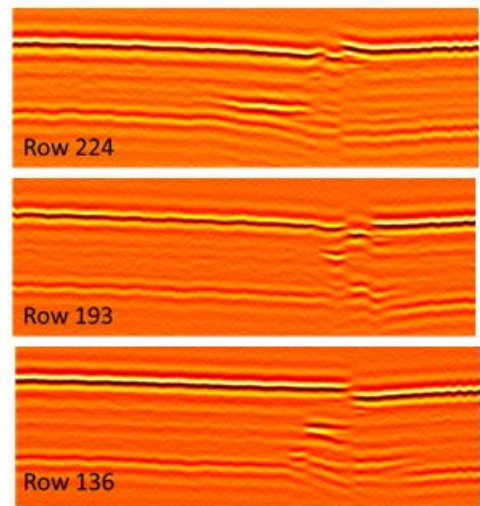
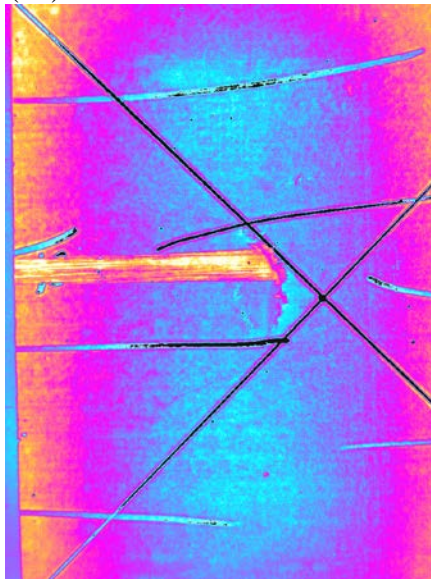
THz signal intensity map (full):



THz internal surface map (zoomed) and row depth scans:

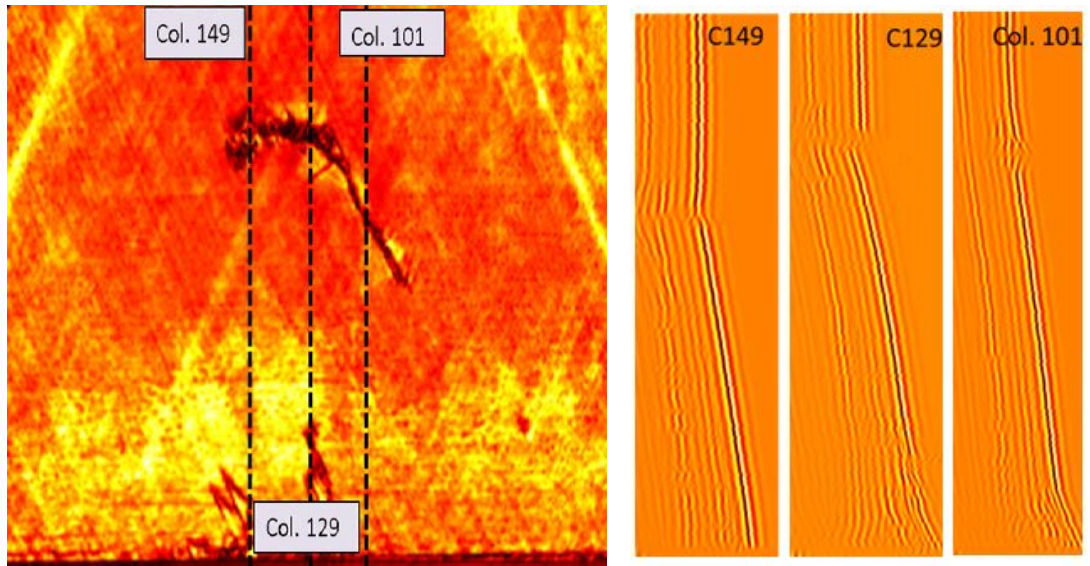


FIRT (1d):

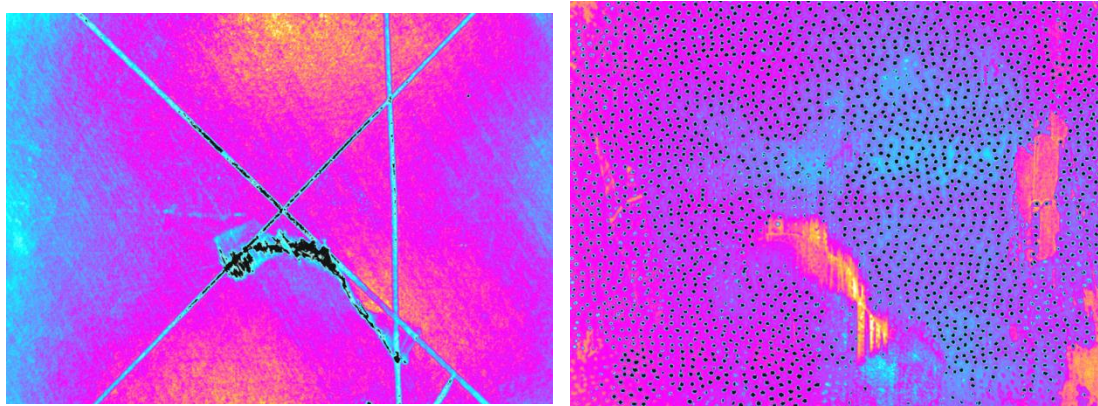


60-1i

THz (signal intensity map, column depth scans):

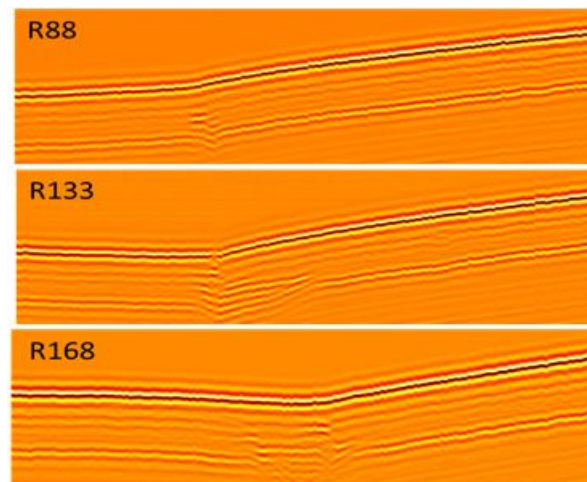
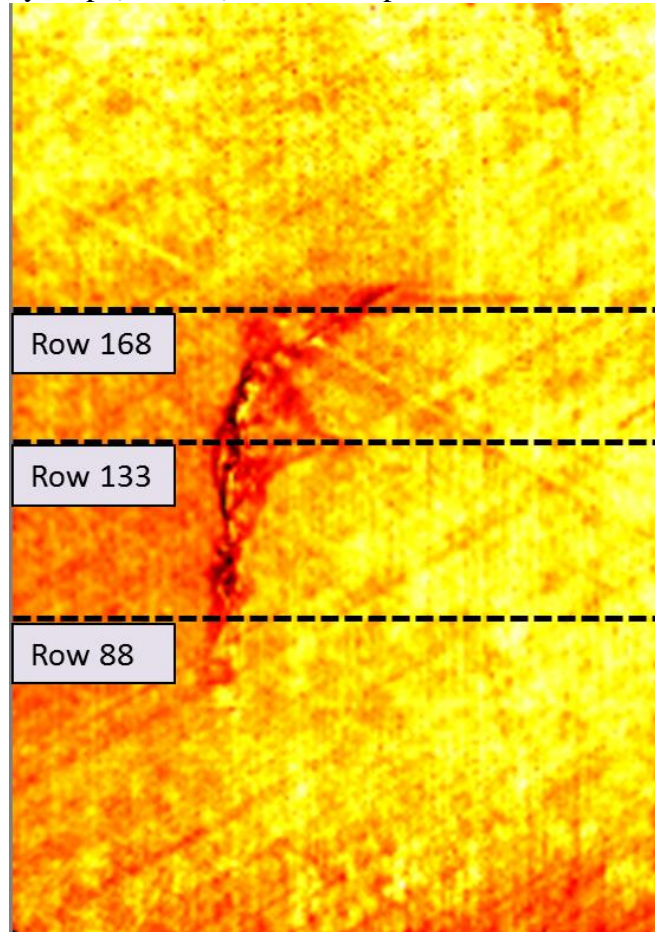


FIRT (front face 1d, back face 1d):



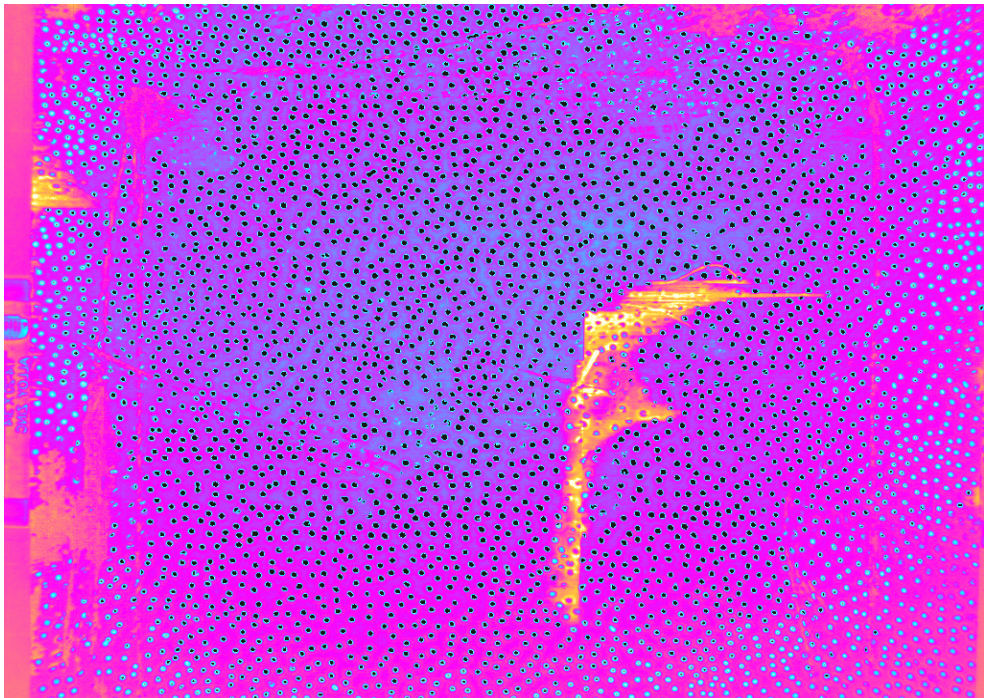
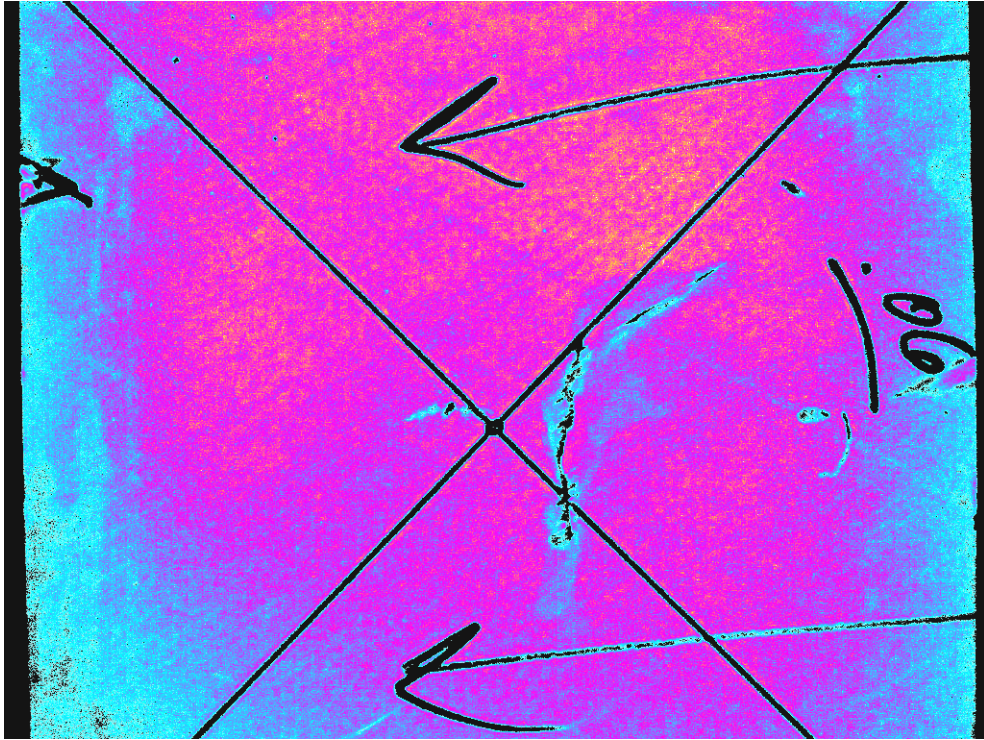
60-2i

THz signal intensity map (zoomed) and row depth scans:



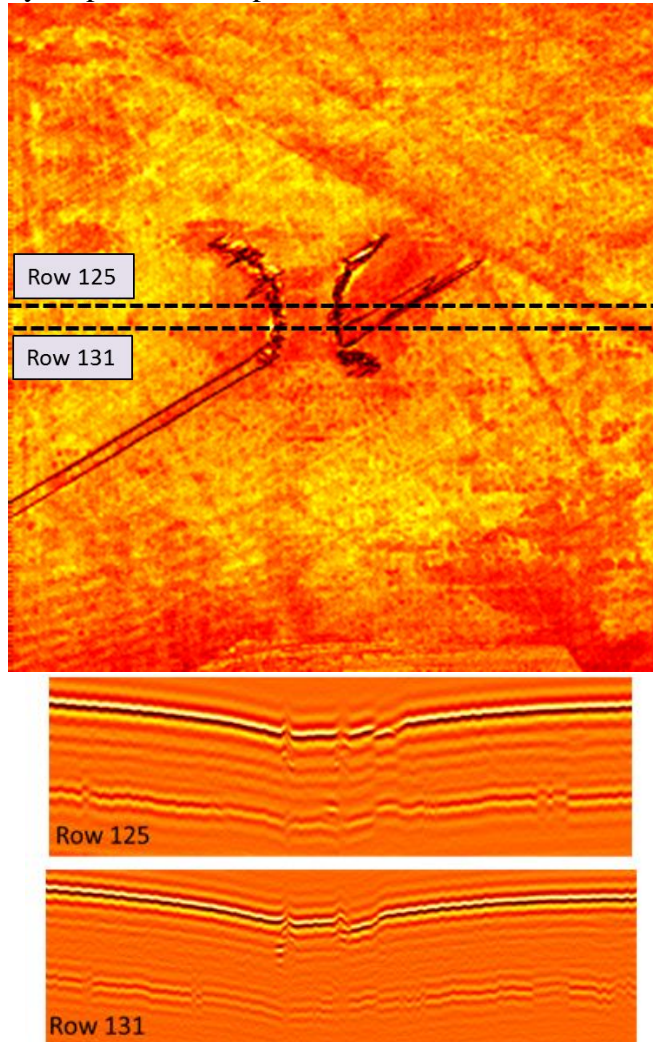
60-2i, continued

FIRT (front and back 1d):

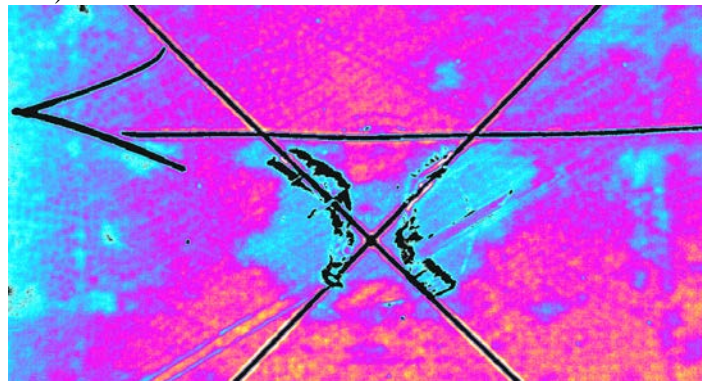


60-4i

THz signal intensity map and row depth scans:

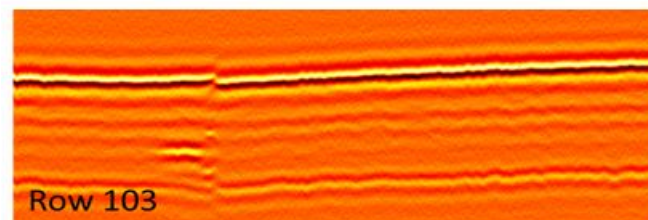
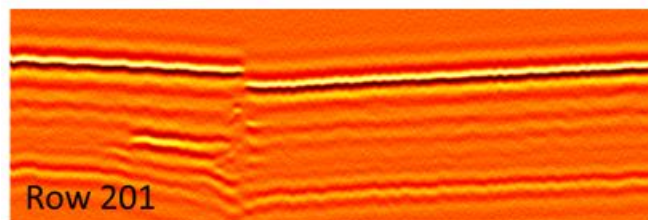
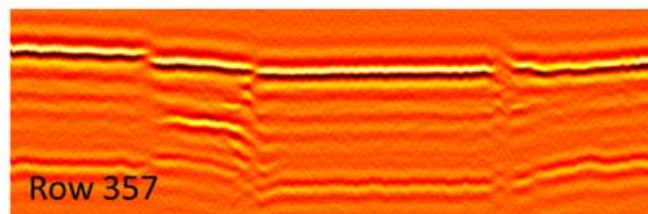
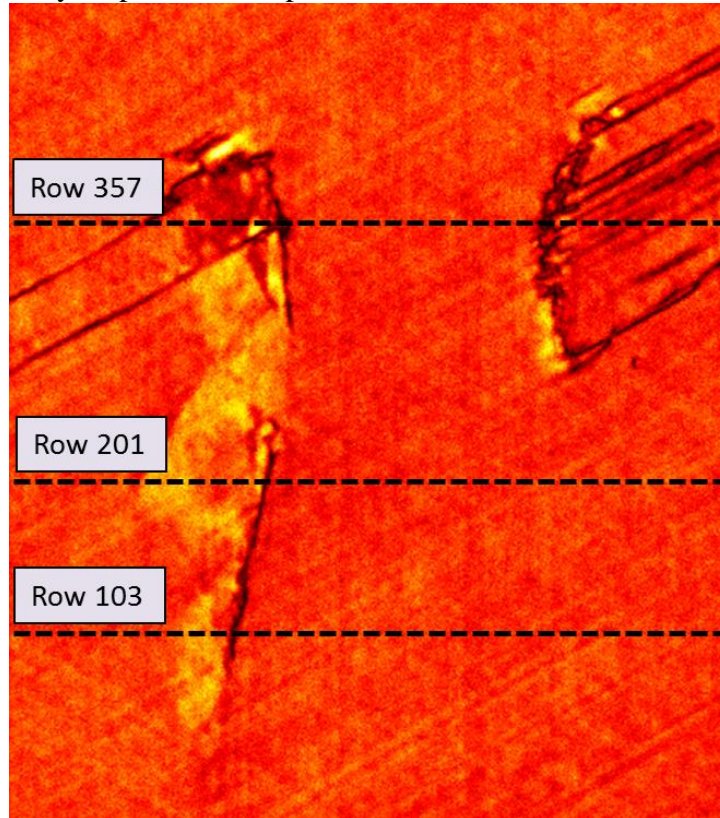


FIRT (front face 1d):



60-7i

THz signal intensity map and row depth scans:



60-7i, continued

FIRT (front face TSR):

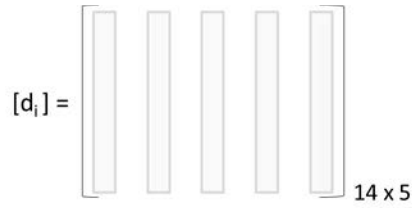


APPENDIX C: ALTERNATIVE METHOD FOR CALCULATING THE COMBINED DAMAGE PARAMETER

In the “Relationship between Damage and Residual Strength” section, a method (Method 1) was provided for deriving a combined damage parameter, $[d_c]$, which combines initially-observed damage quantities, $[d_i]$, with weights based off their correlations to residual strength data. However, not all initially-observed damage quantities are unique, and therefore, only select quantities are needed to create $[d_c]$. In the first method, the significant damage quantities were selected by directly evaluating the correlations between all quantities, and eliminating any redundant quantities.

However, if a large number of initial damage quantities are observed, it may be more challenging to identify which to include in the combined damage parameter, $[d_c]$. Therefore, for more complex damage analyses, an alternative method, Method 2, has been developed using a principal component analysis (PCA) to create the combined damage parameter, $[d_{c, pca}]$. The description below uses this method with the initial five damage quantities as an example, but this method could be used for any amount of initial quantities.

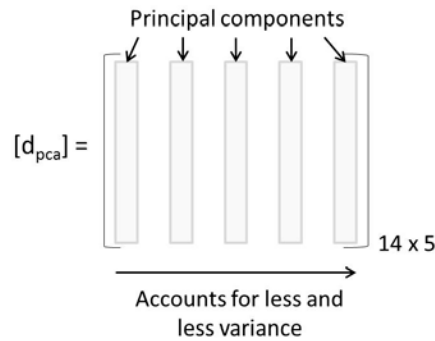
A PCA is a mathematical way of maximizing variance from the raw data—in this case, five damage quantities—to create fewer damage quantities which represent the essence of all initial quantities. A PCA function is well-documented in MATLAB; the inputs to this function are the initial damage vectors $[d_i]$ —in this case, a 14x5 matrix:



$$[coefficients, explained] = PCA(d_i)$$

The PCA function outputs a 5x5 matrix, $[coefficients]$, that when multiplied by the 14x5 matrix $[d_i]$, creates a new 14x5 matrix, $[d_{pca}]$. The columns of $[d_{pca}]$ are the five principal components— five new damage quantities that capture the essence of all initial parameters. Each column accounts for some variance in the data, in decreasing order from left to right.

$$[d_{pca}]_{14 \times 5} = [d_i]_{14 \times 5} * [coefficients]_{5 \times 5}$$



Recall that the goal of the PCA is to reduce the number of damage parameters and maximize variance between them.

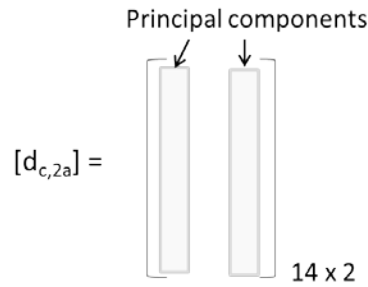
To determine which of the five principal components are significant, the PCA function also returns a matrix, $[explained]$. This 5x1 matrix shows the percentage of variance accounted for by each of the five principal components (columns) of $[d_{pca}]$. For Method 2a, principal components that contribute to at least 1% of the variance are considered to be significant. For this analysis, the $[explained]$ matrix is shown:

$$[explained]_{5 \times 1} = \begin{bmatrix} 86.36 \\ 12.75 \\ 0.88 \\ 0.006 \\ 0.002 \end{bmatrix}$$

Therefore, only the first two principal components account for enough variance to be considered in the combined damage parameter, $[d_{pca}]$. With this, $[d_{pca}]$ can be rewritten as the new combined damage parameter, $[d_{c,2a}]$:

$$[d_{c,2a}]_{14 \times 2} = [d_i]_{14 \times 5} * [coefficients]_{5 \times 2}$$

$$[d_{c,2a}]_{14 \times 2} = [d_i]_{14 \times 5} * \begin{bmatrix} 0.34 & 0.79 \\ 0.85 & -0.02 \\ 0.03 & 0.00 \\ 0.41 & -0.62 \\ 0.02 & -0.02 \end{bmatrix}$$



Now that MATLAB's PCA function has been used to create the combine damage parameter, $[d_{c,2a}]$, a prediction equation can be determined by following the same steps outlined in the "Relationship between Damage and Residual Strength" section of this thesis—starting with Equation 13.

Using Method 2a (the PCA method with two principal components), the compressive residual strength, $\sigma_{R,2a}$, can be predicted by

$$[\sigma_{R,2a}] = m_c * d_{c,2a} + B_c$$

$$= -1.99 * d_{c,2a} + 73.0 \text{ MPa}$$

where $d_{c,2a}$ is defined as

$$d_{c,2a} = \frac{-2.15 * [d_1 \ d_2 \ d_3 \ d_4 \ d_5] \begin{bmatrix} 0.34 \\ 0.85 \\ 0.03 \\ 0.41 \\ 0.02 \end{bmatrix} + 0.09 * [d_1 \ d_2 \ d_3 \ d_4 \ d_5] \begin{bmatrix} 0.79 \\ -0.02 \\ 0.00 \\ -0.62 \\ -0.02 \end{bmatrix}}{-1.73}$$

Method 2a can be used to predict the residual strength of a Cyply 1002 composite laminate with damage quantities determined through visual inspection, FIRT, or THz imaging. The correlation between this prediction equation and the actual residual strength data is -0.8001.

Since the first principal components of $[d_{pca}]$ accounts for 86.36% of the variance as shown in [explained], the analysis was also conducted to eliminate the second principal component, accounting for 12.75% of variance. Method 2b uses only one principal component, whereas Method 2a used two. With Method 2b, the compressive residual strength, $\sigma_{R,2b}$, can be predicted by

$$\begin{aligned} [\sigma_{R,2b}] &= m_c * d_{c,2b} + B_c \\ &= -2.47 * d_{c,2b} + 73.0 \text{ MPa} \end{aligned}$$

where $d_{c,2b}$ is defined as

$$d_{c,2b} = [d_1 \ d_2 \ d_3 \ d_4 \ d_5] \begin{bmatrix} 0.34 \\ 0.85 \\ 0.03 \\ 0.41 \\ 0.02 \end{bmatrix}$$

Method 2b can be used to predict the residual strength of a a Cyply 1002 composite laminate with damage quantities determined through visual inspection, FIRT, or THz

imaging. The correlation between this prediction equation and the actual residual strength data is -0.7987.

The MATLAB code for the principal component analyses is shown in Appendix D.

APPENDIX D: MATLAB CODE FOR DETERMINING PREDICTION EQUATIONS

The following code shows the MATLAB script for:

- Finding the prediction equation presented in the “Relationship between Damage and Residual Strength” section (*Method 1*)
- Finding the prediction equation using the principal component analysis (PCA) as described in Appendix C:
 - with two or more principal components selected (*Method 2a*)
 - with one principal component selected (*Method 2b*)

```

%% All three methods in 1 file

% Method 1: create the combined damage parameter by manually selecting
% parameters 1, 2, and 5
% Method 2a: create the combined damage parameter with the PCA, choosing the
% top 2 contributing principal components.
% Method 2b: create the combined damage parameter with the PCA, choosing the
% top 1 contributing principal component.

%% General for all methods
% Loads all instron data, calculates residual compressive
% strength, identifies which damage parameters are significant using a
% Principal Component Analysis, and creates 1 comprehensive damage
% parameter. With this 1 parameter, creates an equation that can predict
% residual strength given certain damage quantities.

% Panels considered valid: 1ca, 1cb, 1cc, 1ia, 1ib, 2cb, 2ib, 2ic, 4ib,
% 5cb, 5cc, 7ia, 7ib, 7ic

% Puts all 5 damage quantities in to PCA, reduces to 2 damage parameters
% with new coefficients. Uses these parameters to make 1 comprehensive
% damage quantity, which is used to make a prediction equation.

% Import the instron data into MATLAB--> save matrix workspace as
% raw####.mat.
close all
clear all
clc

% Define specimen dimensions for residual strength test
th = 1.524; % thickness mm = 0.06 inches
b = 101.6; % width mm = 4 inches
A = th*b; % cross-sectional area

% Loads all 27 data files (time, ext, load) and damage summary from current directory
files = dir('*.*mat');
for i = 1:numel(files)
    load(files(i).name);
end

% Find maximum time, extension, load, and max compressive force for each specimen:

% 601ca
t_601ca = raw601ca(:,1); e_601ca = raw601ca(:,2)*-1; P_601ca = raw601ca(:,3)*-1; Pmax_601ca =
min(raw601ca(:,3))*-1; % make positive
P_601ca = raw601ca(:,3)*-1; % convert to N
Pmax_601ca =
min(raw601ca(:,3))*-1; % convert to N;
% 601cb
t_601cb = raw601cb(:,1); e_601cb = raw601cb(:,2)*-1; P_601cb = raw601cb(:,3)*-1; Pmax_601cb =
min(raw601cb(:,3))*-1;
% 601cc
t_601cc = raw601cc(:,1); e_601cc = raw601cc(:,2)*-1; P_601cc = raw601cc(:,3)*-1; Pmax_601cc =
min(raw601cc(:,3))*-1;
% 601ia
t_601ia = raw601ia(:,1); e_601ia = raw601ia(:,2)*-1; P_601ia = raw601ia(:,3)*-1; Pmax_601ia =
min(raw601ia(:,3))*-1;
% 601ib
t_601ib = raw601ib(:,1); e_601ib = raw601ib(:,2)*-1; P_601ib = raw601ib(:,3)*-1; Pmax_601ib =
min(raw601ib(:,3))*-1;
% 602cb
t_602cb = raw602cb(:,1); e_602cb = raw602cb(:,2)*-1; P_602cb = raw602cb(:,3)*-1; Pmax_602cb =
min(raw602cb(:,3))*-1;
% 602ib

```

```

t_602ib = raw602ib(:,1);e_602ib = raw602ib(:,2)*-1; P_602ib = raw602ib(:,3)*-1; Pmax_602ib =
min(raw602ib(:,3))*-1;
% 602ic
t_602ic = raw602ic(:,1);e_602ic = raw602ic(:,2)*-1; P_602ic = raw602ic(:,3)*-1; Pmax_602ic =
min(raw602ic(:,3))*-1;
% 604ib
t_604ib = raw604ib(:,1);e_604ib = raw604ib(:,2)*-1; P_604ib = raw604ib(:,3)*-1; Pmax_604ib =
min(raw604ib(:,3))*-1;
% 605cb
t_605cb = raw605cb(:,1);e_605cb = raw605cb(:,2)*-1; P_605cb = raw605cb(:,3)*-1; Pmax_605cb =
min(raw605cb(:,3))*-1;
% 605cc
t_605cc = raw605cc(:,1);e_605cc = raw605cc(:,2)*-1; P_605cc = raw605cc(:,3)*-1; Pmax_605cc =
min(raw605cc(:,3))*-1;
% 607ia
t_607ia = raw607ia(:,1);e_607ia = raw607ia(:,2)*-1;P_607ia = raw607ia(:,3)*-1; Pmax_607ia =
min(raw607ia(:,3))*-1;
% 607ib
t_607ib = raw607ib(:,1);e_607ib = raw607ib(:,2)*-1; P_607ib = raw607ib(:,3)*-1; Pmax_607ib =
min(raw607ib(:,3))*-1;
% 607ic
t_607ic = raw607ic(:,1);e_607ic = raw607ic(:,2)*-1; P_607ic = raw607ic(:,3)*-1; Pmax_607ic =
min(raw607ic(:,3))*-1;

% Define Damage Quantities
delam_edge = damageselect2(:,1).*(25.4); %inches to mm
delam_surf = damageselect2(:,2).*(25.4*25.4); %inches^2 to mm^2
delam_volume = damageselect2(:,3).*(25.4*25.4*25.4); %inches^3 to mm^3
crack_length = damageselect2(:,4).*(25.4); %inches to mm
crack_area = damageselect2(:,5).*(25.4*25.4); %inches^2 to mm^2

% Calculate Residual Compressive Strength, sigmaR_actual in MPa
Pmax = [Pmax_601ca; Pmax_601cb; Pmax_601cc; Pmax_601ia; Pmax_601ib; Pmax_602cb; Pmax_602ib;
Pmax_602ic; Pmax_604ib; Pmax_605cb; Pmax_605cc; Pmax_607ia; Pmax_607ib; Pmax_607ic]; %N
sigmaR_actual = [Pmax_601ca; Pmax_601cb; Pmax_601cc; Pmax_601ia; Pmax_601ib; Pmax_602cb;
Pmax_602ib; Pmax_602ic; Pmax_604ib; Pmax_605cb; Pmax_605cc; Pmax_607ia; Pmax_607ib; Pmax_607ic]./A;
%MPa

% Calculate Correlations
c_delam_edge = corr(delam_edge, sigmaR_actual);
c_delam_surf = corr(delam_surf, sigmaR_actual);
c_delam_volume = corr(delam_volume, sigmaR_actual);
c_crack_length = corr(crack_length, sigmaR_actual);
c_crack_area = corr(crack_area, sigmaR_actual);

%% Method 1
% Using correlations, identify significant damage parameters, [d]
d = [delam_edge delam_surf crack_area]; % mm, mm^2, mm^2

% Normalize chosen correlations, cn, only for the significant parameters [d]
cn_delam_edge = c_delam_edge/(c_delam_surf + c_crack_area + c_delam_edge);
cn_delam_surf = c_delam_surf/(c_delam_surf + c_crack_area + c_delam_edge);
cn_crack_area = c_crack_area/(c_delam_surf + c_crack_area + c_delam_edge);

cn = [cn_delam_edge cn_delam_surf cn_crack_area];

% Calculate slopes, m1, and intercepts, b1, for each parameter [d]
eq_delam_edge = polyfit(delam_edge, sigmaR_actual,1);
eq_delam_surf = polyfit(delam_surf, sigmaR_actual,1);
eq_delam_volume = polyfit(delam_volume, sigmaR_actual,1);
eq_crack_length = polyfit(crack_length, sigmaR_actual,1);
eq_crack_area = polyfit(crack_area, sigmaR_actual,1);

```

```

m1 = [eq_delam_edge(1) eq_delam_surf(1) eq_delam_volume(1) eq_crack_length(1) eq_crack_area(1)];
b1 = [eq_delam_edge(2) eq_delam_surf(2) eq_delam_volume(2) eq_crack_length(2) eq_crack_area(2)]; %MPa

% Create the combined damage parameter, dc
dc1 = abs((m1(1)*cn(1)*d(:,1)) + (m1(2)*cn(2)*d(:,2))+(m1(5)*cn(3)*d(:,3)))/(m1(1)+m1(2)+m1(5));

% Prove that dc correlates better to sigmaR_actual than any initial parameter
c_dc1 = corr(dc1,sigmaR_actual);

% Plot dc_method1 vs sigmaR_actual
FigHandle = figure('Position', [70 70 900 750]); % creates a square box for plotting
hold on
scatter(dc1, sigmaR_actual,'MarkerEdgeColor',[0 0 0],'MarkerFaceColor',[.3 .3 1],'LineWidth',1.0)
box on
xlabel('dc1 (-)')
ylabel('Residual Compressive Strength (MPa)')

% Extract a prediction tool for Method 1. Uses most relevant damage parameters
% to form an equation that could predict residual strength based on combined
% damage mechanisms. Uses the slopes and intercepts of the actual data curve-fit.
mc1 = m1(1)+m1(2)+m1(5);
Bc1 = (b1(1)+b1(2)+b1(5))/3; %averages the y-intercepts from both damage parameters
sigmaR_predict1 =(mc1*dc1)+Bc1; %[MPa]

%% Method 2a
% Principal Component Analysis with top 2 principal components
[coeff,score,latent,tsquared,explained] = pca(damageselect2);

% "Explained" shows the percentage of total variance in data that is
% explained by each of the principal components created by "pca" (aka,
% explained represents the eigenvalues x10). "Coeff" is the eigenvectors.
% Only keep principal factors that explain more than 1% of the total
% variance.
pca_coeffs_2a = [];
for i = 1:5
    if explained(i)>1
        pca_coeffs_2a = [pca_coeffs_2a coeff(:,i)]; % becomes 5x2
    end
end

% Create a matrix of new damage parameters created through PCA to have the
% maximum variance. (Takes all 5 initial parameters, and captures the
% essence of all 5 using only 3 new parameters).
d_pca = damageselect2*pca_coeffs_2a; % creates a 14x2
d1_pca =d_pca(:,1);
d2_pca =d_pca(:,2);

% Define weights from "explained" (based on eigenvalues)
w1 = explained(1)/100;
w2 = explained(2)/100;

%normalize weights to use for total damage parameter
nw = [w1/(w1+w2) w2/(w1+w2)];

% Calculate slopes, m, and intercepts, b, for each principal parameter
eq_d1_pca = polyfit(d1_pca, sigmaR_actual,1);
eq_d2_pca = polyfit(d2_pca, sigmaR_actual,1);
m_individualpcas = [eq_d1_pca(1) eq_d2_pca(1)];
b_individualpcas = [eq_d1_pca(2) eq_d2_pca(2)];

%Create a combined damage parameter, dc2a

```

```

dc2a = ((m_individualpcas(1)*nw(1)*d_pca(:,1)) +
(m_individualpcas(2)*nw(2)*d_pca(:,2)))/(m_individualpcas(1)+m_individualpcas(2));
eq_dc2a = polyfit(dc2a, sigmaR_actual,1);
m2a = eq_dc2a(1);
b2a = eq_dc2a(2);

% Create a prediction tool from Method 2a. Uses the total damage quantity created by the PCA
% to form an equation that could predict residual strength based on combined
% damage mechanisms. Uses the slopes and intercepts of the actual data curve-fit.

sigmaR_predict2 = (m2a*dc2a) + b2a;

% Prove that dc2a correlates better to sigmaR_actual than d1_pca or d2_pca or
% any of 5 initial parameters
c_d1_pca = corr(d1_pca, sigmaR_actual);
c_d2_pca = corr(d2_pca, sigmaR_actual);
c_dc2a = corr(dc2a,sigmaR_actual);

% Plot prediction tool versus actual data
FigHandle = figure('Position', [70 70 900 750]); % creates a square box for plotting
hold on
scatter(dc2a, sigmaR_actual,'MarkerEdgeColor',[0 0 0],'MarkerFaceColor',[1 .5 1],'LineWidth',1.0)
box on
xlabel('dc2a(-)')
ylabel('Residual Compressive Strength (MPa)')

%% Method 2b
% Principal Component Analysis with top 1 principal component
pca_coeffs_2b = [];
for i = 1:5
    if explained(i)>15
        pca_coeffs_2b = [pca_coeffs_2b coeff(:,i)]; % becomes 5x1
    end
end

%Create a combined damage parameter, dc2b
dc2b = damageselect2*pca_coeffs_2b;
eq_dc2b = polyfit(dc2b, sigmaR_actual,1);
m2b = eq_dc2b(1);
b2b = eq_dc2b(2);

% Create a prediction tool from Method 2b. Uses the best principal component
% from PCA
sigmaR_predict2 = (m2b*dc2b) + b2b;

% Prove that dc2b correlates better to sigmaR_actual than any of 5 initial parameters
c_dc2b = corr(dc2b,sigmaR_actual);

% Plot prediction tool versus actual data
FigHandle = figure('Position', [70 70 900 750]); % creates a square box for plotting
hold on
scatter(dc2b, sigmaR_actual,'MarkerEdgeColor',[0 0 0],'MarkerFaceColor',[1 .5 1],'LineWidth',1.0)
box on
xlabel('dc2b(-)')
ylabel('Residual Compressive Strength (MPa)')

```

BIBLIOGRAPHY

- Arora, H., Kelly, M., Worley, A., Del Linz, P., Fergusson, A., Hooper, P. A., & Dear, J. P. (2014, May). Compressive strength after blast of sandwich composite materials. *Philosophical Transactions. Series A, Mathematical, Physical, and Engineering Sciences*. <https://doi.org/10.1098/rsta.2013.0212>
- ASTM D3039/D3039M-17 Standard Test Method for Tensile Properties of Polymer Matrix Composite Materials. (2017). West Conshohocken, PA: ASTM International. https://doi.org/https://doi.org/10.1520/D3039_D3039M-17
- ASTM D3410/D3410M-16 Standard Test Method for Compressive Properties of Polymer Matrix Composite Materials with Unsupported Gage Section by Shear Loading. (2016). West Conshohocken, PA: ASTM International. https://doi.org/https://doi.org/10.1520/D3410_D3410M-16
- ASTM D7137/D7137M-17 Standard Test Method for Compressive Residual Strength Properties of Damaged Polymer Matrix Composite Plates. (2017). West Conshohocken, PA: ASTM International,. https://doi.org/https://doi.org/10.1520/D7137_D7137M-17
- ASTM D7264/D7264M-15 Standard Test Method for Flexural Properties of Polymer Matrix Composite Materials. (2015). West Conshohocken, PA: ASTM International. https://doi.org/https://doi.org/10.1520/D7264_D7264M-15
- Badiger, S. M. (2004). Design and Fabrication of an Experimental Facility for Controlled, Transient Shock Wave Loading. University of Rhode Island.

- F. Adams, D., A. Carlsson, L., & Pipes, R. B. (2003). *Experimental Characterization of Advanced Composite Material (Third)*. CRC Press.
- Farley, G. L. (1985). Effect of low-velocity or ballistic impact damage on the strength of thin composite and aluminum shear panels. National Aeronautics and Space Administration, Scientific and Technical Information Branch.
- Kannan, V. K., Rajadurai, A., & Rao, B. N. (2011). Residual strength of laminated composites after impact. *Journal of Composite Materials*, 45(9), 1031–1043. <https://doi.org/10.1177/0021998310378904>
- Koo, J.-M., Choi, J.-H., & Seok, C.-S. (2013). Evaluation for residual strength and fatigue characteristics after impact in CFRP composites. *Composite Structures*, 105, 58–65. <https://doi.org/10.1016/J.COMPSTRUCT.2013.05.004>
- Kumar, P., LeBlanc, J., Stargel, D. S., & Shukla, A. (2012). Effect of plate curvature on blast response of aluminum panels. *International Journal of Impact Engineering*, 46, 74–85. <https://doi.org/10.1016/J.IJIMPENG.2012.02.004>
- LeBlanc, J. (2005). *Experimental Evaluation of Novel Composites for Use in Transport of Explosive Materials*. University of Rhode Island.
- LeBlanc, J., Shillings, C., Gauch, E., Livolsi, F., & Shukla, A. (2016). Near Field Underwater Explosion Response of Polyurea Coated Composite Plates. *Experimental Mechanics*, 56(4), 569–581. <https://doi.org/10.1007/s11340-015-0071-8>
- LeBlanc, J., Shukla, A., Rousseau, C., & Bogdanovich, A. (2007). Shock loading of three-dimensional woven composite materials. *Composite Structures*, 79(3), 344–355. <https://doi.org/10.1016/J.COMPSTRUCT.2006.01.014>

- Lockhart, P. (2015). Terahertz Imaging Nondestructive Maintenance Inspections (Distribution Statement A). Naval Undersea Warfare Center Division, Newport.
- Pettit, D. E., Lauraitis, K. N., Cox, J. M., & BURBANK., L.-C. C. O. (1979). Advanced Residual Strength Degradation Rate Modeling for Advanced Composite Structures. Volume 1. Task I: Preliminary Screening. Defense Technical Information Center. Retrieved from <https://books.google.com/books?id=9mCiAQAACAAJ>
- Ruiz, A. (1997). Residual Strength After Fatigue of a Cross-Ply Metal Matrix Composite at Elevated Temperature. AIR FORCE INST OF TECH WRIGHT-PATTERSON AFB OH. Retrieved from <http://www.dtic.mil/docs/citations/ADA327989>
- Saether, E. (2001). RESTRAN: Residual Strength Analysis of Impact Damaged Composite Laminates Volume I: Theoretical Manual.
- Schreier, H., Orteu, J. J., & Sutton, M. A. (2009). Image correlation for shape, motion and deformation measurements: Basic concepts, theory and applications. Image Correlation for Shape, Motion and Deformation Measurements: Basic Concepts, Theory and Applications. <https://doi.org/10.1007/978-0-387-78747-3>
- Shukla, A., & Dally, J. W. (2014). Experimental Solid Mechanics (Second). Knoxville, TN: College House Enterprises, LLC. Retrieved from <https://books.google.com/books?id=W8ijoAEACAAJ>